The Frankfurt Biosphere Model: a global process-oriented model of seasonal and long-term CO_2 exchange between terrestrial ecosystems and the atmosphere. I. Model description and illustrative results for cold deciduous and boreal forests

Matthias K. B. Lüdeke, Franz-W. Badeck, Ralf D. Otto, Christof Häger,
Silke Dönges, Jürgen Kindermann, Gudrun Würth, Torsten Lang, Ulrich Jäkel,
Axel Klaudius, Peter Ramge, Stefan Habermehl, Gundolf H. Kohlmaier

Institut für Physikalische und Theoretische Chemie, J. W. Goethe-Universität Frankfurt am Main, Marie-Curie-Str. 11,
D-60439 Frankfurt am Main, Germany

ABSTRACT· Within the global carbon cycle the world's ecosystems are most sensitive to environmental change. We present a global model for calculating the seasonal pattern of uptake and release of CO_2 by vegetation and soil in a steady-state climate simulation as well as the long-term development in a changing environment. Within the terrestrial ecosystems 32 vegetation types are distinguished and combined with 7 distinct soil types with respect to their water-holding capacities. Within each vegetation type the living biomass is divided into 2 compartments, one with a short (seasonal) turnover containing the photosynthesizing tissue, feeder roots, and assimilate store, and the other with a long turnover mainly consisting of structural plant material. The mathematical description is based on 2 hypotheses: (1) vegetation tends to maximize photosynthesizing tissue; and (2) a minimum amount of structural tissue is needed to support and maintain the productive parts, described by an allometric relation. The fluxes are modeled using standard equations for gross photosynthesis of the canopy, autotrophic respiration, and decomposition of dead organic matter depending on surface temperature, soil moisture, and irradiation. Within the system of differential equations the free parameters for each vegetation type are calibrated on the basis of a characteristic seasonal climate. In this paper the results of steady-state climate experiments for the 2 vegetation types 'cold deciduous forest' and 'boreal forest' are compared with ecological measurements. It was shown that the model yields satisfactory results with respect to phenology, gradients in net primary production, and standing biomass and thus holds the promise to also yield good global results.

KEY WORDS: Carbon balance · Terrestrial ecosystems · Global simulation model · Allocation and phenology · Primary production · CO_2 exchange fluxes

The metamorphosis of plants calls to our attention a dual law: (1) the law of the internal nature by which plants are constituted; (2) the law of the external circumstances by which plants are modified. (Johann Wolfgang von Goethe 1790)

INTRODUCTION

Changes in trace gas and particulate composition of the atmosphere are assumed to be one of the main causes for the variation of the global climate during the last 150 yr. Since the beginning of industrialization the atmospheric mixing ratio of carbon dioxide has increased from 280 to 350 ppmv and continues to rise at a rate of 0.45 % per year (Keeling et al. 1989) mainly due to burning of fossil fuel, and deforestation and other changes in land use. In the same period the mixing ratio of methane rose from 0.7 to 1.7 ppmv and continues to rise at a rate of 1.0 % per year (Rasmussen & Khalil 1986). To understand the mechanisms of this rise

and its consequences, it is important to investigate the global carbon cycle, namely the fluxes among the biosphere, the lithosphere, the oceans, and the atmosphere.

The atmospheric retention of carbon dioxide is determined by oceanic uptake and the concurrent storage or release in deep-sea waters, by exchange fluxes in terrestrial ecosystems, and by storage in living as well as dead biomass. These global fluxes and changes in pool sizes, up to now, could not be addressed by direct measurements, leaving mathematical modeling and computer simulations as the main tools for analysis. Due to the uncertainty of the effects to be incorporated and the parameter values to be used, there is still a high level of uncertainty in the results of these models.

The coupling of models on atmospheric transport with those on oceanic as well as terrestrial biotic exchange fluxes, with the aim of comparing the output of such coupled models with measured atmospheric carbon dioxide concentration fields, can be regarded as an important means of evaluating model results. The Frankfurt Biosphere Model (FBM) has been developed for simulations with coupled models in the context of a European Research Project (EPOCH) and a German National Climate Research Program.

The role of terrestrial biota within the global carbon cycle is still not completely understood. Positive and negative feedbacks must be taken into consideration with respect to the interaction of vegetation and climate. Stimulation of ecosystem production by atmospheric trace constituents and effects of temperature and precipitation changes play an important role in this interaction.

Despite the large extent of tropical deforestation, the terrestrial biosphere as a whole still seems to have a stabilizing effect on atmospheric CO_2 content, e.g. as proposed by Kohlmaier et al. (1991). Results from indirect modeling of the seasonal and regional distribution of atmospheric CO_2 (Enting & Mansbridge 1989, Tans et al. 1990) seem to corroborate this hypothesis, indicating that terrestrial biota in the mid-latitudes of the northern hemisphere are an important sink for atmospheric CO_2. This hypothesis has been supported lately by a compilation of data on forest productivity (Heath et al. 1993). Further evidence of enhanced assimilation rates stems from analyzing the amplitude of the seasonal CO_2 signal (Kohlmaier et al. 1989).

The fertilization effect of increased atmospheric carbon dioxide on plant production has been addressed in the past by several model attempts with high aggregation levels in either time or space or both (e.g. Esser 1987, Kohlmaier et al. 1990, Gifford 1992). Since the expression of a CO_2 fertilization effect is a complex function of temperature (Farquhar et al. 1980, Long & Drake 1992) and moisture availability, it is desirable to

account for changes in regional climatic conditions, all the more as GCM (General Circulation Model) results indicate that a future greenhouse climate will include high latitudinal and altitudinal variability.

Positive and negative feedbacks are to be expected from temperature effects on the balance of assimilation and respiration fluxes, as well as from changes in water availability. Especially a possible melting of permafrost soils and sinking water tables in peatlands are expected to result in increased methane and carbon dioxide releases to the atmosphere (Gorham 1991). Additionally, exchange fluxes may change under episodic climatic conditions. Carbon-13 data, for example, seem to indicate that excess CO_2 is released from the land biota in El Niño years in which the CO_2 in the atmosphere follows a distinctive seasonal pattern (Keeling et al. 1989).

From this the conclusion may be drawn that modeling the interaction of internal vegetation dynamics and climatic driving variables will capture some major traits of carbon exchanges in terrestrial ecosystems. Tight links between climate and vegetation have already established the basis for numerous scientific approaches in the past.

In climatology and paleoclimatology, information on vegetation distribution has been used to reconstruct climatic gradients. The distribution of pollen and other fossil records as well as special anatomical traits have served as climate indicators, as evidence (proxy data) of climate (Schwarzbach 1974).

Climatic data have been used to predict dominant vegetation types or life zones based on temperature and moisture limitations for different life forms (Holdridge 1947, Box 1981, Woodward 1987, Prentice et al. 1992).

The correlation between climatic variables and ecosystem performance has been determined from regression analysis (Box & Meentemeyer 1991). Applying the correlation between productivity and precipitation as well as annual mean temperature determined by Lieth (1975), a regionalized simulation of the net primary production for the world's ecosystems has been performed (Esser 1991).

In the last decade there has been some progress in integrating knowledge on the climatic limits of life forms with mechanistic models for aspects of ecosystem mechanisms in order to predict additional vegetation characteristics in climatic gradients. For example, Woodward (1987) presented a model for the prediction of LAI (leaf area index) calculated on the basis of a water balance model.

Several global models on the carbon exchange fluxes have been developed in the past, comprising highly aggregated dynamic models (e.g. Moore et al. 1979, Kohlmaier et al. 1987), models based predomi-

nantly on relations derived from regression analysis (e.g. Esser 1991), and models based on remote sensing data (e.g. Heimann & Keeling 1989, Ruimy 1991). At present there is a process underway to close the gap between global and ecosystem (stand-level) models. In the scope of these modeling efforts special attention has been paid to the impacts of climate at the global level (Esser 1987) as well as for single vegetation stands (Running & Coughlan 1988). Recently, Melillo et al. (1993) published global results of a Terrestrial Ecosystem Model (TEM; Raich et al. 1991) with high resolution in time and space compared to earlier global carbon cycle models but still with high aggregation on temporal as well as spatial scales compared to stand-level models. The model presented here has similar intermediate spatial resolution but higher temporal resolution, paying special attention to the internal dynamics of carbon in the living biomass. It especially addresses prognoses of seasonal fluxes resulting from these dynamics.

These climatic effects and additional effects (changing frequencies of natural fires, altered vegetation periods, determinants of agriculture, etc.) will result in a spatially variable pattern of changing climatic conditions, affecting the annual cycle of carbon storage and release. It is therefore desirable to develop models with high spatial and temporal resolution. Additionally, the models should allow for a very process-orientated description of the underlying physiology because of the complex response functions mentioned above. For these reasons, we at first developed a model describing climatic impacts, being aware of the fact that edaphic factors, such as nutrient availability, have a substantial impact as well, which deserve more exact description than in this version of the model. The aims of the current model can be characterized as follows:

– Describe the seasonal pattern of uptake and release of CO_2 by vegetation and soil in a steady-state climate experiment.

– Describe processes of time developments within ecosystems considering the observable age class distributions.

– Describe the differences in CO_2 exchange between the normal reference year and a chosen El Niño period, e.g. the ENSO (El Niño - Southern Oscillation) event of 1982/1983.

– Describe the long-term development of terrestrial biota from the beginning of industrialization to the present considering climate change as well as land-use changes.

– Perform a series of prognostic experiments into the next 50 or 100 years using the experiments mentioned above to calibrate the model parameters.

– Perform experiments coupled with ocean and climate models.

To meet these aims the model should fulfill the following requirements:

– The model should include the major processes responsible for the reaction of the different ecosystem types to climatic variations and be as simple as possible in order to be manageable at a global scale.

– The time resolution should be in the range of hours/days in order to examine the effects of climate as they are described by relatively detailed physiological models

– The representation of the variety of the world's ecosystems requires a high spatial resolution. Commonly used vegetation maps (soil maps) assign a limited number of ecosystem types (soil types) to a 1° × 1° or 0.5° × 0.5° latitude/longitude grid.

– The characteristic properties of these ecosystem types should be expressed in terms of (measurable) quantities like standing biomass, net photosynthesis, net primary production (NPP), soil carbon density, etc.

– The major ecophysiological processes of CO_2 uptake and release should be photosynthesis, autotrophic, and heterotrophic respiration.

– The main variables driving the processes mentioned above should be light intensity, temperature, and precipitation (and in a further state of development, CO_2 concentration). Additionally, soil fertility and water storage capacity should be taken into account as major driving forces.

MODEL STRUCTURE

Here we present the compartmentalization together with the corresponding definition of carbon and water fluxes and the carbon allocation model, which do not depend on the particular modeling of the fluxes. Equations expressing the dependence of the fluxes on climate and compartment sizes are then explained.

Compartmentalization

For each ecosystem type we propose the same basic model structure, comprising the presumably minimal subdivision of the total carbon content of the living biomass (BC) into 2 compartments, according to Janecek et al. (1989). We distinguish between the parts of the vegetation with a short turnover time (leaves, feeder roots and stored assimilates, summarized in the GC compartment) and mostly woody, structural material with a long turnover time (RC compartment). The letters G and R refer to green and remaining biomass, which were distinguished in the original version. Now leaf biomass is assumed to be a constant fraction of the GC compartment. To describe the decomposition
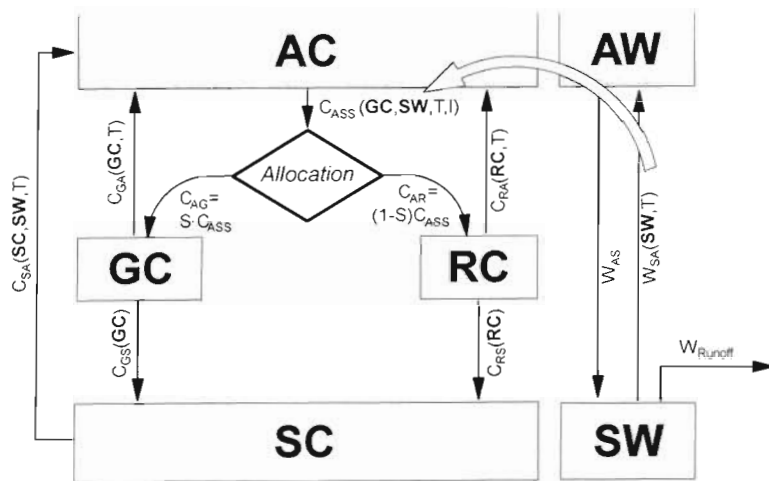
Fig. 1 Flow chart and model structure. Symbols with 2 letters represent reservoirs of carbon (second letter C) and water (second letter W): AC, atmospheric carbon; GC, carbon content of green biomass and feeder root biomass plus assimilate store; RC, carbon content of remaining biomass of biota; SC, carbon content of litter, humus and dead biomass; AW, water in the atmosphere; SW, soil water in the rooting zone. C and W: carbon and water fluxes; indices indicate sources and sinks of these fluxes, and the functional dependence of the fluxes on the driving variables and pool sizes is given in parentheses (T: hourly air temperature; I: hourly photosynthetic active radiation, PAR). W_{AS}: daily precipitation; W_{SA}: daily actual evapotranspiration; S: fraction of total assimilation C_{ASS} allocated to GC

processes a 1-compartment model for dead organic matter after Fung et al. (1987) is used (carbon mass of litter and humus are summarized in the soil carbon SC compartment). Furthermore the soil water compartment SW is introduced to calculate the actual status of soil water. Carbon and water fluxes among these compartments and the atmosphere A generally depend on climatic variables and pool sizes, both varying in time (Fig. 1). This structure is assumed to be sufficient to describe the major carbon uptake and release processes in any grid element representing the terrestrial surface, the advantage is the limited and constant number of parameters required. Hence the local difference of the model source and sink strength is influenced externally by climatic variables and internally by vegetation properties, assumed to be reflected by the state of the system and suitable parameter values.

Carbon allocation and phenology

As shown in Fig. 1 it is assumed that the assimilate production C_{ASS} is determined by the carbon mass of compartment GC, reflecting the amount of leaves, by the actual soil water content SW, and by the external driving variables temperature T and irradiation I. This flux is partitioned according to the present needs of plant organs, namely the growth and the maintenance of photosynthesizing tissue and feeder roots (represented by GC) on the one hand, and the growth and maintenance of stems, branches, and roots (represented by RC) on the other. Furthermore, assimilates which are translocated into particular storage organs are included in the carbon-mass of the GC compartment as well.

The partitioning of the carbon assimilation flux C_{ASS} into the GC and RC compartments in seasonal and long-term patterns is derived from some basic assumptions:

It is possible to identify 'forbidden' regions in the state space of vegetation (GC-RC plane). These forbidden states (GC, RC) are characterized by RC-values which are too small to support and maintain the given amount of leaves contained in the GC compartment. The minimum amount of RC fulfilling the functional requirements of the organs represented by GC will be called $\Omega(GC)$. Because it is not yet possible to determine this value by explicit modeling, data from field measurements were used (Reichle 1981). Experimental findings and theoretical considerations suggest that a parabola type of function, the so-called allometric relation, is a suitable parametrisation (see Janecek et al. 1989).

$$RC = \Omega(GC) = \xi \cdot GC^{\kappa} \qquad (1)$$

For the functional types temperate broadleaved forest, coniferous forest, tropical evergreen forest, and grasslands, measurements of woody and/or structural biomass as well as the maximum leaf mass (extrapolated on the total mass of the GC compartment) were used to determine the parameters in Eq. (1) by least-squares fitting. Typical courses of $\Omega(GC)$ for woody vegetation are shown in Fig. 2. The parameter κ was kept constant for all vegetation types which were assigned to functional types mentioned above, while ξ was calculated separately for each particular vegetation type using the characteristic climax values GC_{max} and RC_{max}:

$$\xi = \left(\frac{RC_{max}}{GC_{max}} \right)^{\kappa} \qquad (2)$$

Vegetation tends to maximize the amount of photosynthesizing tissue. This implies that the system allocates most of the assimilates into the GC compartment until the trajectory reaches the confinement of the region of allowed states, $RC = \Omega(GC)$, maximizing its potential production. When $\Omega(GC)$ is reached the
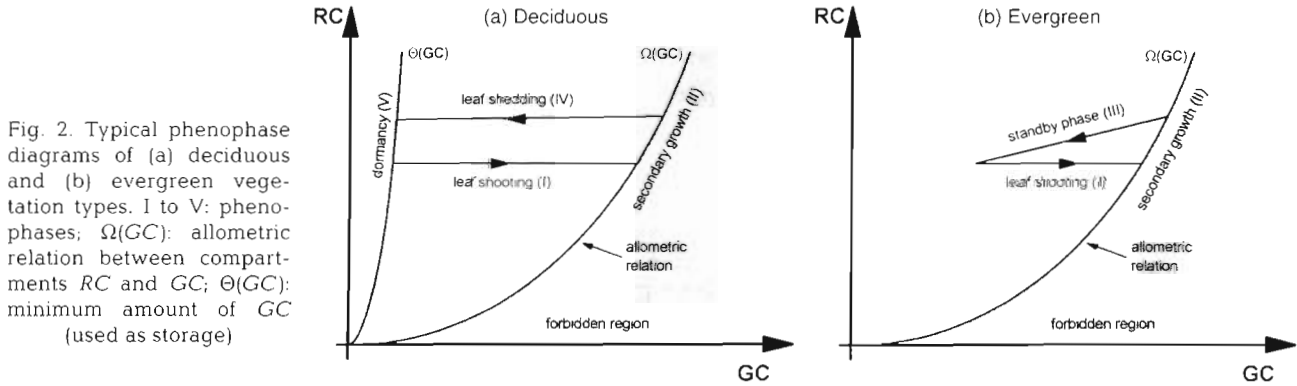
Fig. 2. Typical phenophase diagrams of (a) deciduous and (b) evergreen vegetation types. I to V: phenophases; $\Omega(GC)$: allometric relation between compartments RC and GC; $\Theta(GC)$: minimum amount of GC (used as storage)

growing system is forced to allocate simultaneously to the GC and RC compartments to avoid the forbidden region of the GC-RC plane.

Evergreen and deciduous vegetation need to be distinguished. It is necessary to distinguish at least 2 phenotypes according to their behavior during the phase where no net growth is possible. In the case of evergreen vegetation the allocation ensures an equilibrated net loss of biomass from the GC and RC compartments whereas for deciduous vegetation an active process of leaf abscission is started resulting in a complete cessation of carbon assimilation out of the vegetation period.

From these assumptions follow the allocation strategy for the evergreen vegetation type during the whole year and the strategy for the deciduous type during the vegetation period. To formalize the qualitative statements above we introduce an allocator S, $0 \leq S \leq 1$ (Table 1), which represents the fraction of assimilate to be allocated into the GC compartment. With this, we obtain the balance equations for the changes in GC and RC (Table 1).

Two additional phenophases need to be considered for the deciduous type outside of the vegetation period. At the begining of a season in which weather conditions do not allow for biomass increase (drought or cold) a leaf abscission phase reduces the GC compartment to a remaining amount of feeder roots and assimilate store. This amount is assumed to be proportional to the annual maximum of GC and is characterized by the function (see Fig. 2a)

$$RC = \Theta(GC) = v \cdot GC^{\varkappa} \tag{3}$$

When the trajectory reaches this curve (by leaf shedding) the dormancy phase starts. During this phase the biomass losses, as defined by RC respiration and the total litter production, $C_{BS} = C_{RS} + C_{GS}$, are distributed among the compartments such that the systems trajectory follows the $\Theta(GC)$ curve. This phase ends when weather conditions allow net biomass increase under the assumption of the total conversion of stored assimilates into leaf biomass and feeder roots. These additional phases are described by the differential equations in Table 2. The assimilate allocation is described

Table 1. Differential equations for phases I, II, and III

$$\frac{dGC}{dt} = S \cdot C_{ASS} - C_{GA} - C_{GS} \qquad \frac{dRC}{dt} = (1-S) \cdot C_{ASS} - C_{RA} - C_{RS}$$

Phase	Allocator (S)	Description
I	$S = \dfrac{C_{ASS} - C_{RA}}{C_{ASS}}$	Shooting phase: all assimilates are allocated into GC except a flux for the compensation of RC respiration
II	$S = \dfrac{C_{ASS} + \dfrac{d\Omega}{dGC} \cdot (C_{GA} + C_{GS}) - (C_{RA} + C_{RS})}{\left(1 + \dfrac{d\Omega}{dGC}\right) \cdot C_{ASS}}$	Secondary growth phase: allocation ensures simultaneous growth of the GC and RC compartment. The systems trajectory equals $RC = \Omega(GC)$. For the detailed derivation of S see Appendix 1A
III	$S = \dfrac{C_{GS} + C_{GA}}{C_{GS} + C_{GA} + C_{RS} + C_{RA}}$	Standby phase: this phase allows for a balanced decrease of GC and RC

Table 2. Differential equations for phases IV and V

Phase	Differential equations	Description
IV	$$\frac{dGC}{dt} = -\frac{\Omega^{-1}(RC) - \Theta^{-1}(RC)}{\tau_{IV}}$$ $$\frac{dRC}{dt} = -C_{RA} - C_{RS}$$	Leaf shedding phase: during leaf abscission leaf metabolism is assumed to be neglectable. Once started, this phase ends independently of the driving variables when the trajectory reaches the curve $RC = \Theta(GC)$
V	$$\frac{dGC}{dt} = \frac{1}{1 + \dfrac{d\Theta}{dGC}} \cdot (-C_{RA} - C_{BS})$$ $$\frac{dRC}{dt} = \frac{\dfrac{d\Theta}{dGC}}{1 + \dfrac{d\Theta}{dGC}} \cdot (-C_{RA} - C_{BS})$$	Dormancy phase: respiration and litter losses are distributed such that the systems trajectory equals $RC = \Theta(GC)$. For the detailed derivation see Appendix 1B

in terms of photosynthesis (C_{ASS}), a representation we chose in order to stay close to the biological process. On the other hand a more concise formulation for phases II and V (yielding exactly the same results) can be derived by formulating the allocation of NPP ($C_{ASS} - C_{GA} - C_{RA}$), which was done in earlier models on the global carbon cycle (Goudriaan & Ketner 1984).

For a given state (GC, RC) of living vegetation, particular weather conditions, and a given phenotype, Table 3 gives the conditions to determine the actual phenophase. For convenience, the net biomass change ΔBC and ΔBC_{cold} (water limitation is neglected) are introduced:

$$\Delta BC = C_{ASS} - C_{GA} - C_{GS} - C_{RA} - C_{RS} \tag{4}$$

In phase V C_{ASS} stands for the potential assimilation.

Together with the dependence of the fluxes on the state and weather variables (see section 'Calculation of carbon and water fluxes') the equations given in Tables 1, 2 & 3 define the short- and long-term dynamics of the carbon pools in living biomass.

The simple conditions given in Table 3 are sufficient to determine the actual phenophase (i.e. the valid differential equation) depending on weather and state of development as long as the course of the driving vari-

ables during the year is smooth. This holds for all calculations presented in this paper where the daily values of the driving variables are derived by interpolation of monthly averages of temperature and precipitation. To drive the model with less smooth weather inputs, Table 3 must be modified with respect to deciduous vegetation, while the conditions for the evergreen phenotype are still valid. These modifications are documented in Appendix 1C.

Dynamics of the soil compartments

According to Fig. 1 we obtain from the balance of fluxes the following differential equations for the soil carbon compartment SC and the soil water compartment SW:

$$\frac{dSC}{dt} = C_{GS} + C_{RS} - C_{SA} \tag{5}$$

$$\frac{dSW}{dt} = W_{AS} - W_{SA} - W_{Runoff} \tag{6}$$

In the model presented here, Eq. (6) is decoupled from the time development of the carbon pools. Hence, the soil water model can be run prior to the carbon model. Starting with the field capacity the soil

Table 3. Conditions determining the actual phenophase

Phase I (deciduous and evergreen)	Phase II (deciduous and evergreen)	Phase III (evergreen)	Phase IV (deciduous)	Phase V (deciduous)
$\Delta BC > 0$ ∧ $RC > \Omega(GC)$	$\Delta BC > 0$ ∧ $RC = \Omega(GC)$	$\Delta BC \leq 0$ –	starts: $\Delta BC_{cold} \leq 0$ ∧ $RC < \Theta(GC)$	$\Delta BC \leq 0$ ∧ $RC = \Theta(GC)$

water model is run until a stable annual course of soil water is established. In a future model coupling will be incorporated via the dependence of the actual evapotranspiration W_{SA} on the actual amount of leaves, represented by a fraction of the GC compartment.

Calculation of carbon and water fluxes

The net uptake of CO_2 by plants is determined by a balance of 2 processes: carbon assimilation, C_{ASS} (i.e. the gross photosynthetic carbon fixation) and autotroph respiration, C_{GA} and C_{RA}. As assimilation and respiration show different seasonal courses and different temperature responses we think it is more appropriate to model these processes separately rather than directly simulating NPP.

Uptake of CO_2

The effective carbon assimilation rate, C_{ASS}, can be considered as a product function of a term h_1 dependent on light and canopy structure, a temperature dependent term h_2, and a soil water dependent term h_3.

$$C_{ASS} = \alpha \cdot LAI(GC) \cdot h_1(I, LAI(GC)) \cdot h_2(T) \cdot h_3(SW) \quad (7)$$

The dependence on light intensity and leaf area index, LAI, is modeled by the approach of Monsi & Saeki (1953), with $LAI = \frac{1}{2} SLA\ GC$ assuming that the leaf carbon mass is half the carbon mass of the GC compartment. The conversion factor SLA (specific leaf area) is determined for each vegetation type.

At the individual leaf level in the canopy the light dependence of the production is chosen to be of the Michaelis-Menten type:

$$C_{ASS}^{(leaf)} = \alpha \cdot \frac{I_{can}(L)}{K_1 + I_{can}(L)} \cdot h_2(T) \cdot h_3(SW) \quad (8)$$

where L is the cumulative leaf area index, with $0 \leq L \leq$ LAI. $I_{can}(L)$ is the incident photosynthetically active radiation, PAR, within the canopy, while α is the production at light saturation and soil water and temperature optimum ($h_2 = h_3 = 1$).

It is advantageous for a global model with several vegetation types to replace K_1 by the ratio of α and Φ, in which the initial quantum yield, Φ [$\Phi = (\partial C_{ASS}/\partial I_{can})_{I_{can}=0}$], is taken to be a universal constant for C3 and C4 plants respectively:

$$C_{ASS}^{(leaf)} = \alpha \cdot \frac{I_{can}(L)}{\frac{\alpha}{\Phi} + I_{can}(L)} \cdot h_2(T) \cdot h_3(SW) \quad (9)$$

In Monsi & Saeki's model the incoming light is attenuated in the canopy according to Beer's law:

$$I_{can}(L) = I \cdot e^{-k \cdot L} \quad (10)$$

where k is the extinction coefficient of the canopy and I denotes PAR above the canopy.

Canopy assimilation is obtained by integration of Eq. (9) over all leaf layers using Eq. (10). Assuming temperature and soil water limitation being independent of crown depth, we get:

$$C_{ASS} = \alpha \cdot h_2(T) \cdot h_3(SW) \int_0^{LAI} \frac{I \cdot e^{-k \cdot L}}{\frac{\alpha}{\Phi} + I \cdot e^{-k \cdot L}} dL \quad (11)$$

$$= \frac{\alpha}{k} \cdot \ln \left(\frac{\frac{\alpha}{\Phi} + I}{\frac{\alpha}{\Phi} + I \cdot e^{(-k \cdot LAI)}} \right) \cdot h_2(T) \cdot h_3(SW)$$

From Eq. (11) the maximum canopy production ($I \to \infty$; $h_2 = h_3 = 1$) can be calculated as $\alpha \cdot LAI$. Normalization leads to:

$$h_1 = \frac{1}{\alpha \cdot LAI} \cdot C_{ASS} = \frac{1}{k \cdot LAI} \cdot \ln \left(\frac{\frac{\alpha}{\Phi} + I}{\frac{\alpha}{\Phi} + I \cdot e^{(-k \cdot LAI)}} \right) \quad (12)$$

As mentioned above the processes of assimilation and autotroph respiration are described separately due to their different responses to temperature. However, the temperature dependence of the *gross* photosynthesis for the different ecosystems cannot be derived directly from physiological measurements whereas for the *net* photosynthesis, C_{CER}, the cardinal points minimum, optimum, and maximum temperatures, T_{min}, T_{opt}, and T_{max}, are given by Larcher (1980). The shape of the corresponding curve is often approximated by a fractional rational function ranging between 0 and 1 (e.g. Raich et al. 1991):

$$f(T) = \frac{(T - T_{min}) \cdot (T - T_{max})}{(T - T_{min}) \cdot (T - T_{max}) - (T - T_{opt})^2}. \quad (13)$$

Given the function for the temperature dependence of net photosynthesis or carbon exchange rate respectively, C_{CER}, and the function for the temperature dependence of autotroph respiration, C_{GA}, Eq. (18) plus the parameter values T_{min}, T_{opt}, and T_{max}, the temperature dependence of gross photosynthesis, $h_2(T)$, is determined by the equality:

$$C_{CER}(I, GC, T, SW) = C_{ASS} - C_{GA} \quad (14)$$
$$= \alpha \cdot LAI\ h_1(I, GC) \cdot h_2(T) \cdot h_3(SW) - \beta \cdot GC \cdot e^{\omega(T - T_0)}$$

As the measurements of T_{min}, T_{opt}, and T_{max} were performed under optimal conditions with respect to light and moisture, Eq. (14) reduces to:
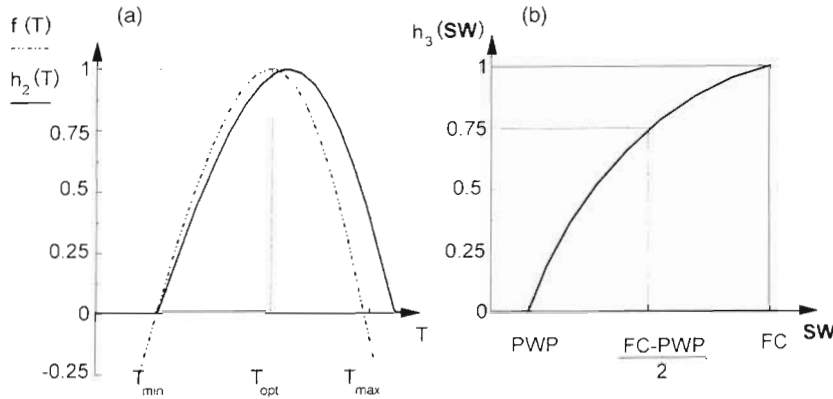
Fig. 3. (a) Dependence of gross photosynthesis, $h_2(T)$, and leaf net photosynthesis, $f(T)$, on temperature. (b) Dependence of assimilation on soil water content

$$C_{CER}(GC,T) = GC \cdot \left\{ \alpha \frac{SLA}{2} \cdot h_2(T) - \beta \cdot e^{\omega(T-T_0)} \right\} \quad (15)$$

Since the term in parentheses on the right side of Eq. (15) is proportional to $f(T)$ it can be equated to the product of $f(T)$ and an arbitrary constant a_T. Solving for h_2 leads to:

$$h_2(T) = \frac{2}{\alpha \cdot SLA} \cdot \left\{ a_T \cdot f(T) + \beta \cdot e^{\omega(T-T_0)} \right\} \quad (16)$$

The constant a_T can be determined numerically from the condition that at its maximum the function $h_2(T)$ should be equal to 1. For temperature values, where $h_2(T)$ would become negative, h_2 is set equal to 0 (see Fig. 3a).

The dependence of C_{ASS} on water availability, represented by the soil water content SW is modeled with an empirical relation:

$$h_3(SW) = \frac{\tanh\left(a_{SW} \dfrac{SW - PWP}{FC - PWP} \right)}{\tanh(a_{SW})}; \quad 0 \le h_3(SW) \le 1 \quad (17)$$

The edaphic parameters field capacity, FC, and permanent wilting point, PWP, denote properties depending on soil type (Appendix 3). The factor a_{SW} is chosen such that for a relative soil moisture content of 50 % $h_3(SW) = 0.75$ as proposed by Larcher (1980) and shown in Fig. 3b. This reflects the evidence that plant production is not or only little affected as long as the soil water content is close to field capacity whereas at lower levels of soil water a stronger decrease in plant production is observed.

Release of CO₂-autotroph respiration

Autotroph respiration is modeled similarly for both compartments GC and RC, depending on the corresponding compartment size and an exponential func-

tion of the temperature:

$$C_{GA} = \beta \cdot GC \cdot e^{\omega(T-T_0)} \quad (18)$$

and

$$C_{RA} = \gamma \cdot RC \cdot e^{\omega(T-T_0)} \quad (19)$$

where β and γ are parameters to be determined by calibration and $T_0 = 293$ K is the reference temperature where β and γ directly reflect the rate constants. The parameter ω depends on vegetation type and is related to the common Q_{10} values by

$$\omega = \frac{1}{10} \cdot \ln Q_{10} \quad (20)$$

Litter production

Woody litter production is assumed to be proportional to the RC compartment:

$$C_{RS} = \delta \cdot RC \quad (21)$$

Litter production of the GC compartment for evergreen types is modeled with the same functional form:

$$C_{GS}(\text{evergreen}) = \varepsilon \cdot GC \quad (22)$$

For deciduous types the litter production of the GC compartment occurs during the abscission phase (IV). Its rate is calculated as the constant fraction $1/\tau_{IV}$ of the horizontal distance between the allometric relations $\Omega(GC)$ and $\Theta(GC)$

$$C_{GS}(\text{deciduous}) = \frac{\Omega^{-1}(RC) - \Theta^{-1}(RC)}{\tau_{IV}} \quad \text{(phase IV)} \quad (23)$$

In the present version τ_{IV} is set to 30 d (Dixon 1976, Ellenberg et al. 1986).

During the dormancy phase (V) the total litter production is assumed to be proportional to the standing biomass

$$C_{BS}(\text{deciduous}) = \delta \cdot (GC + RC) \quad \text{(phase V)} \quad (24)$$

Release of CO_2 — heterotroph respiration

The decomposition of dead organic matter in our model depends on temperature and soil moisture. For the temperature response we use the same concept as Fung et al. (1987) who distinguish 4 respiration groups ($RG = 1,...,4$). However, in addition we consider the dependence on compartment size and soil moisture as introduced above for the net assimilation. For temperate/boreal needle leaved ($RG = 3$) and broad leaved vegetation ($RG = 2$) this leads to:

$$C_{SA} = \begin{cases} \eta \cdot h_3(SW) \cdot (1 + q_{RG}\ T) \cdot SC & \text{for } q_{RG} \cdot T > -1 \\ 0 & \text{otherwise} \end{cases} \quad (25)$$

Fung et al. (1987) suggested describing the tropical/subtropical woody vegetation ($RG = 1$) and grasslands ($RG = 4$) by a linear regression of the reduced temperature T/T_{max}. Following this approach for these vegetation types we describe the heterotrophic respiration by

$$C_{SA} = \begin{cases} \eta \cdot h_3(SW) \cdot \left(1 + q_{RG} \cdot \dfrac{T}{T_{max}}\right) \cdot SC & \text{for } q_{RG} \cdot \dfrac{T}{T_{max}} > -1 \\ 0 & \text{otherwise} \end{cases} \quad (26)$$

with q_{RG} as given by Fung et al. (1987). In both cases T is given in °C and η is a normalization factor.

Water fluxes

The actual evapotranspiration, W_{SA}, is calculated by the product of potential evapotranspiration, W_{PET}, and the soil-water dependent function h_3 as used in the calculation of assimilation because of the close relation between assimilation and transpiration.

$$W_{SA} = W_{PET}\ h_3(SW) \quad (27)$$

The potential evapotranspiration, W_{PET}, is calculated using the procedure of Thornthwaite (1948) who found an empirical relation between potential evapotranspiration and temperature, modified by the annual temperature course.

The use of $h_3(SW)$ for the determination of photosynthetic water limitation (Eq. 7) and the calculation of actual evapotranspiration implies a linear relationship between these 2 fluxes. This is a first crude approximation which should be modified in the course of an improved representation of plant-water interactions.

Runoff, W_{Runoff}, comprises both surface runoff and drainage in our model. It is not explicitly calculated but taken as the surplus water when the soil water content reaches field capacity (soil water content staggered between permanent wilting point and field capacity).

The input flux, W_{AS}, into the soil water compartment SW represents daily precipitation.

DRIVING VARIABLES AND PARAMETERS

Climatic input data

The current version of the FBM uses Shea (1986) as data source for long-term average climate. This database contains 1 annual cycle of monthly average air temperature and monthly sum of precipitation averaged over the years 1950 to 1979 and interpolated to a 2.5° × 2.5° latitude/longitude grid. This data base was extrapolated to a 1° × 1° grid. We derived daily values by distributing the monthly average temperature and precipitation sum, respectively, smoothly over 1 month using the procedure described in Appendix 1D.

Daylength and hourly values of photosynthetic active radiation (PAR) were calculated according to Richter (1985) (see Appendix 1D). For a future version of FBM a procedure has been developed to calculate atmospheric attenuation of PAR based on cloudiness data as for instance given by Leemans & Cramer (1991).

Vegetation and soil maps

As a basis of our vegetation map we chose a 1.0° × 1.0° spatial resolution for 32 different types of potential vegetation (29 types excluding water, desert, ice and cultivated land) as collected by Matthews (1983). A closer examination and comparison of certain grid elements with vegetation maps provided by UNESCO/FAO (1969), Schmidthüsen (1976), UNESCO (1981), and Olson & Watts (1982) reveal some problematic assignments in the Matthews system. For instance, vegetation type 1, 'tropical evergreen forest, mangrove forest', extends far beyond the western border of the Amazonian basin. In this and other cases of unrealistic assignments we ascribed other vegetation types than those of Matthews. Additionally the classification of shrublands and grasslands was changed according to Schmidthüsen (1968, 1976) considering the distribution of C3 and C4 grasses. We chose as a lower bound for the predominance of C4 plants a maximum monthly mean temperature of 22 °C and a minimium monthly mean temperature of −1 °C. The modified vegetation map distinguishes 32 vegetation types (see Appendix 2).

To calculate the dynamics of soil water content, it is necessary to know the available water capacity (field

capacity – wilting point, AWC) of the soil. To get this capacity for every grid element, we used the global soil map compiled by Wilson & Henderson-Sellers in 1985. This map, based on FAO/UNESCO (1974), has a $1° \times 1°$ resolution and gives 21 different categories. Three classes of color (light, medium, dark), texture (coarse, medium, fine) and drainage (good, impeded, poor) are distinguished (Appendix 3). Omitting the classification of color, the occurring combinations of texture and drainage are mapped on field capacity and wilting point, assuming an average rooting depth of 1 m.

Ecological parameters

Ecological and ecophysiological parameters required for the application of the set of equations described above and for the calibration procedure have been determined from the literature.

Parameters referring to the sizes of carbon pools

For the mean climax biomass of any of the vegetation types in Matthews' (1983) vegetation map under typical climate conditions, we use the parameter values compiled by Matthews (1984). The partitioning of the total biomass, BC, on the maximum annual climax pool sizes of the GC and RC compartments (GC_{max}, RC_{max}) respectively was derived from Rodin et al. (1972), Larcher (1980), Schulze (1982), and Medina & Klinge (1983).

For the vegetation types added during the reconciliation of the distribution and classification of vegetation after Matthews (1983, 1984), we determined parameter values following Rodin et al. (1972), Lieth (1975), Schulze & Kappen (1975), Ajtai et al. (1979), Hadley & Szarek (1981), Ehleringer & Mooney (1983), Walter & Breckle (1983, 1984, 1986, 1991), and Long et al. (1992). The parameters ξ and κ defining the allometric relation were determined by curve fitting to biomass data obtained from several sources (Janecek et al. 1989) with the additional condition that $RC_{max} = \Omega(GC_{max})$.

Specific leaf area (SLA) has been fixed according to the data for typical leaf area indices (LAI) compiled by Kira (1975), Whittaker & Likens (1975), and Schulze (1982) and the climax leaf biomasses. The ratio of leaf and feeder root biomass subject to modelation as a function of nutrient availability has been fixed to 1:1 as a first order approximation.

The organic carbon contents of soils, SC_{max}, have been chosen according to the data reported by Atjai (1979), Schlesinger (1984), and Post et al. (1985).

Parameters referring to carbon fluxes in the climax state

For the mean value of net primary productivity, NPP, in the climax state we adopted the parameter values given by Fung et al. (1987), which are assigned to every biome type of Matthews' vegetation map. GPP was calculated from NPP according to the ratios of both fluxes reported by Kira (1975), Lieth (1975), Larcher (1980), and Medina & Klinge (1983).

The annual integral of the autotroph respiration fluxes in the climax state $ResG$ and $ResR$, which equals $GPP - NPP$ by definition, is assumed to be partitioned in equal parts onto the respiration of the GC and RC compartments, as reported for an oak forest in Wisconsin, USA (Reichle 1981).

The annual integral of the rate of leaf litter production LpG is determined from leaf longevity for evergreen vegetation types. For deciduous vegetation types the additional parameter v for the left state space confinement $\Theta(GC)$ is calculated from an estimate of the storage pool derived from the data on biomass and phenology reported in Ellenberg et al. (1986).

Parameters for the respiration functions

The carbon release due to the decomposition of the humus layer is modeled according to Fung et al. (1987).

The parameter ω determining the temperature dependence of autotrophic respiration of the GC as well as the RC compartments has been derived from typical Q_{10} values for several functional vegetation units reported by Ryan (1991).

Vegetation type specific minimal, maximal, and optimal temperatures T_{min}, T_{max}, and T_{opt} of net photosynthesis were adapted from Larcher (1980).

Parameters describing the light attenuation and light response

The absorption coefficient, k, for the Lambert Beer formula was adopted from Larcher (1980) and Jarvis & Leverenz (1983). We use 2 different parameter values for the initial quantum yield, Φ, in C3 and C4 plants according to the results reported by Björkmann (1981).

Soil parameters

The soil map of Wilson & Henderson-Sellers (1985) provides texture, drainage, and color classes. To each combination of texture and drainage we assigned field capacities, FC, and permanent wilting points, PWP

Table 4. Parameter sets for vegetation types 8 and 11

Parameter	Type 8	Type 11
GC_{max} (kg C m^{-2})	1.62	0.25
RC_{max} (kg C m^{-2})	11.8	12.35
SC_{max} (kg C m^{-2})	14.0	12.0
NPP (kg C m^{-2} yr^{-1})	0.585	0.54
$ResG$ (kg C m^{-2} yr^{-1})	0.29	0.27
$ResR$ (kg C m^{-2} yr^{-1})	0.29	0.27
LpG (kg C m^{-2} yr^{-1})	0.53	0.18
T_{min} (K) (°C)	270.6 (−2.6)	273.2 (0)
T_{max} (K) (°C)	311.6 (38.5)	313.2 (40)
T_{opt} (K) (°C)	290.6 (17.5)	294.2 (21)
k (−)	0.5	0.5
Φ (kg C J^{-1})	2.56×10^{-09}	2.56×10^{-09}
SLA (m^2 kg C^{-1})	12	40
ω (K^{-1})	0.0833	0.0833
RG (−)	3	2
q_{RG} (°C^{-1})	0.07	0.16
κ (−)	1.6	1.6
ξ [(kg C m^{-2})$^{1/\kappa}$]	5.49	112.04
v [(kg C m^{-2})$^{1/\kappa}$]	−	769.1
τ_{IV} (d)	−	30
ΔT (K)	8	8

(Appendix 3) neglecting the color of the soil. Values for FC and PWP were taken from the 'Water' Yearbook of Agriculture, USDA 1955 (Donahue et al. 1977) and Clapp & Hornberger (1978).

Parameter sets for the boreal evergreen needle leaved forests (vegetation type 8) and the cold deciduous broad leaved forests (vegetation type 11) are given in Table 4.

CALIBRATION

Characteristic climate

Starting from the fact that there is a strong correlation between climate and vegetation type, we interpreted the vegetation-type dependent data for typical annual net primary production and typical annual autotrophic respiration as follows. The integrals of the seasonal fluxes (e.g. C_{ASS}, C_{GA} and C_{RA}) represent yearly values (GPP, $ResG$, $ResR$), produced by an average climate course which is characteristic for the respective vegetation type.

To determine this characteristic climate of a vegetation type we started with the seasonal (monthly values, $m = 1,...,12$) course of temperature T, precipitation P (Shea 1986) and irradiation I at all sites i ($i = 1,...,N$) where the particular vegetation type is found. A simple geographical average over the climate variables would not yield a reliable characteristic climate because the phase shifts between the grid elements would cause a

strong underestimation of the typical seasonality of the signal. In order to solve this problem of phase quenching when averaging climatic signals being out of phase, we first shifted all time courses of the southern hemisphere grid elements by 6 mo as

$$m = \begin{cases} m_{North} & \text{northern hemisphere} \\ 1 - mod_{12}(m_{South} + 5) & \text{southern hemisphere} \end{cases} \quad (28)$$

in which the function $mod_{12}(n)$ returns the remainder of n divided by 12.

Then the month of the maximum of the climate variable, $m_{X,max}(i)$, is determined in each grid element i, where X stands for temperature T, precipitation P, or irradiation I. Next, the mean month of the maximum of X of the whole vegetation type, $m_{X,max}^{char}$, is determined as the value resulting in the minimum mean-square deviation from all $m_{X,max}(i)$ values. This procedure ensures that the average of, for instance, December and February will be January rather than July, which would be the result of the arithmetic mean. Finally the characteristic climate course is calculated by averaging the single grid element climate courses which are now shifted in time so that all maxima are located at $m_{X,max}^{char}$:

$$X_{char}(m) = \frac{1}{N} \cdot \sum_{i=1}^{N} X(m_X, i), \quad \text{for } X = T, P, I \quad (29)$$

where

$$m_X = 1 + mod_{12}(m + 11 + m_{X,max}(i) - m_{X,max}^{char}) \text{ for } X = T, P$$

$$m_X = m \qquad \qquad \text{for } X = I$$

This procedure preserves (1) the typical phase relations between temperature, light and precipitation (reflecting characterizations like e.g. 'winter rain') and (2) the typical amplitude of the annual course of climate variables.

In Fig. 4 the characteristic climate course for the temperate/subpolar evergreen needleleaved forests (vegetation type 8) is displayed.

Determination of model parameters and calibration runs

The remaining vegetation-type dependent free parameters in the flux equations (defined in 'Model structure — Calculation of carbon and water fluxes'), represent the maximum photosynthesis rate per leaf area, α, and the rate coefficients β, γ, δ, ε, and η for the respiration and litter production fluxes. The idea of the FBM calibration procedure is to chose these parameters in such a way that a 1 yr equilibrium model run,

started at (GC_{max}, RC_{max}) and driven by the characteristic climate as calculated in the preceeding section, yields annual values for gross primary production, GPP, autotroph respiration, $ResG$ and $ResR$, litter production, LpG, etc., given in Table 4.

The following equations describe the calibration conditions which determine the 5 free parameters for the deciduous vegetation types (α, β, γ, δ, η) and the 6 free parameters for the evergreen vegetation types (α, β, γ, δ, ε, η) respectively:

(1) Gross primary production, GPP:

$$GPP = NPP + ResG + ResR \qquad (30)$$
$$= \int_0^{1\,yr} C_{ASS}(\alpha, GC(t), I(t), T(t), SW(t))\, dt$$

(2) Autotrophic respiration of GC compartment, ResG:

$$ResG = \int_0^{1\,yr} C_{GA}\big(\beta, GC(t), T(t)\big)\, dt \qquad (31)$$

(3) Autotrophic respiration of RC compartment, ResR:

$$ResR = \int_0^{1\,yr} C_{RA}\big(\gamma, RC(t), T(t)\big)\, dt \qquad (32)$$

(4) Litter production of RC compartment, LpR:

$$LpR = NPP - LpG = \int_0^{1\,yr} C_{RS}\big(\delta, RC(t)\big)\, dt \qquad (33)$$

(4a) Litter production LpG of the GC compartment (only for evergreen types):

$$LpG = \int_0^{1\,yr} C_{GS}(\varepsilon, GC(t))\, dt \qquad (34)$$

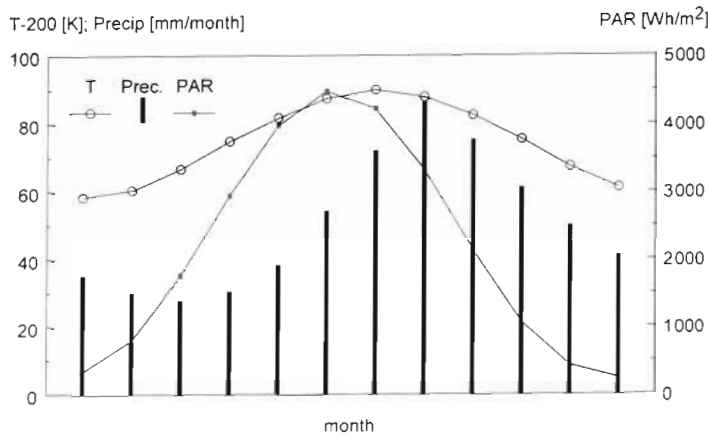T-200 [K]; Precip [mm/month]   PAR [Wh/m²]

Fig. 4. Characteristic climate of a temperate/subpolar evergreen needleleaved forest (vegetation type 8)

Table 5. Table of calibrated parameters for vegetation types 8 and 11

Parameter	Type 8	Type 11
α (kg C m^{-2} s^{-1})	2.82×10^{-08}	5.92×10^{-08}
β (s^{-1})	1.77×10^{-08}	3.20×10^{-08}
γ (s^{-1})	2.35×10^{-09}	1.96×10^{-09}
δ (s^{-1})	1.33×10^{-10}	9.41×10^{-10}
ε (s^{-1})	1.10×10^{-08}	–
η (s^{-1})	1.44×10^{-09}	1.11×10^{-09}

(5) Heterotrophic respiration of the SC compartment, assuming a steady state, ResS:

$$ResS = NPP = \int_0^{1\,yr} C_{SA}(\eta, SC(t), T(t), SW(t))\, dt \qquad (35)$$

This problem cannot be solved analytically, as these conditions together with the model equations form a set of coupled integro-differential equations. However, the parameters (α, β, γ, δ, ε, η) can be calculated by means of an interactive and iterative numerical procedure. During this iteration the parameters are adjusted until the target values (left sides of the conditions stated above) are met simultaneously with a given precision.

Because there is no vegetation feedback on the water cycle in the present state of the model, it is possible to simplify the calibration procedure by calculating the equilibrium time course of $SW(t)$ for the given characteristic climate in advance. To perform this we first calculated the area-weighted average permanent wilting point, PWP_{char}, and field capacity, FC_{char}, for each vegetation type. With these values the soil water model runs until a stable seasonal cycle of the soil water content is established.

Table 5 shows the results of the calibration procedure for vegetation types 8 and 11. The calculated value of α is within the observed range of photosynthetic capacity of tree leaves of 3 to 8 µmol m^{-2} s^{-1} for dominant deciduous tree species and 2 to 3 µmol m^{-2} s^{-1} for *Picea abies*, as the characteristic tree species in the boreal needle leaved forests (Ceulemans & Saugier 1991) (5.92×10^{-8} kg C m^{-2} s^{-1} = 4.9 µmol m^{-2} s^{-1}, 2.82×10^{-8} kg C m^{-2} s^{-1} = 2.4 µmol m^{-2} s^{-1}). However, one should be careful with identifying the parameter α with measured values for single leaves because of the crude representation of the canopy structure (leaf angle distribution, intracanopy gradient in assimilation capacity, etc.). Nevertheless, the deviation should not exceed a factor of 2. Thus, the good agreement between observation and

the result of the calibration procedure supports in our opinion the valid approach of this model.

On the other hand the calibration parameter for wood turnover, δ, for vegetation type 8 reveals the need for a reconciliation of the ecological parameters. The value of 1.33×10^{-10} s^{-1} is too low by a factor of 4.

RESULTS

To illustrate the properties of the model presented above we discuss 2 equilibrium runs, for vegetation types 8 (temperate/subpolar evergreen needleleaved forest) (Fig. 5) and 11 (cold deciduous forest) (Figs. 6 & 7), driven by the climate data given by Shea (1986). The numerical integration of the model equations was performed using 1 d timesteps (assuming a relatively slow variation of the compartment sizes) while the calculation of the daily carbon fluxes was done on a hourly basis, using the daily time courses of the driving variables as given in Appendix 1D. The model was run until the difference between NPP and annual litter fall was <5 g. The vegetation type dependent parameters defining the model equations are given in Tables 4 & 5.

Net primary production and biomass

The model outlined above predicts a total NPP of 5.4 Gt C yr^{-1} for the world's boreal forests and 2.5 Gt C yr^{-1} for the cold deciduous forests excluding mixed forests. The simulation was terminated in the steady state, i.e. the results represent ecosystems in the climax. Figs. 5 & 6 show the net primary production for vegetation types 8 and 11 respectively. The high NPP of the coniferous forests in the western Pacific part of North America is often documented in the literature and is also simulated by the model. A gradient from high NPP values in the south to very low values in the north can be explicitly seen in both figures in the regional NPP distribution in Alaska (type 8) and in East Asia (type 11). In Great Britain and Ireland the simulated NPP has values greater than 0.6 kg C m^{-2} yr^{-1} caused by the influence of the Gulf Stream.

The standing biomass for the boreal forests is predicted to total 126 Gt C; for the cold deciduous forests a total of 57 Gt C is predicted.

In comparison, the Terrestrial Ecosystem Model (TEM) predicts a total NPP of 2.9 Gt C yr^{-1} for boreal forests and of 2.2 Gt C yr^{-1} for cold deciduous forests (Melillo et al. 1993). Differences for boreal forests can be traced back to parameters determining mean productivity, i.e. calibration NPP in FBM and maximum rate of C assimilation, C_{max}, in TEM. In the simulation run presented here the mean productivities for boreal

and cold deciduous forests, as adapted from Fung (1987), are approximately identical (0.585 and 0.54 kg C m^{-2} yr^{-1} respectively). In contrast, in TEM the maximum rate of assimilation for boreal forests is only about half of that for deciduous forests (676.2 and 1207.9 g C m^{-2} mo^{-1}). This difference in the relation of the parameters determining the mean level of assimilation can be identified as the reason for the difference in total NPP of boreal forests in FBM and TEM simulations.

Variability in climate and soil properties determining the soil water status is the sole cause of the variability in NPP and biomass in different locations of a given vegetation type in the current version of our model. In Fig. 8 we show the frequency distribution of the net primary production for both vegetation types. The resulting distributions only approximately match Gaussian normal distributions.

The mean NPP for the boreal forests is 0.555 kg C m^{-2} yr^{-1} compared with the calibration parameter of 0.585 kg C m^{-2} yr^{-1}. Most of the 1436 grid elements (98.3%) range in primary productivity between 0.2 and 0.8 kg C m^{-2} yr^{-1}. The standard deviation is 0.133 kg C m^{-2} yr^{-1}. For deciduous forests the respective values of NPP are 0.491 kg C m^{-2} yr^{-1} for the mean and 0.540 for the calibration parameter. In this vegetation type 99.9% of the grid elements have a net primary production between 0.1 and 0.8 kg C m^{-2} yr^{-1}, with a standard deviation of 0.183 kg C m^{-2} yr^{-1}.

The variability in these results is similar to the output reported by TEM for comparable vegetation types. The boreal forests in TEM exhibit a mean NPP of 0.238 kg C m^{-2} yr^{-1}, a maximum of 0.434 and a minimum of 0.124 kg C m^{-2} yr^{-1}. In temperate deciduous forests the respective results are 0.620 kg C m^{-2} yr^{-1} for the mean, maximum 0.978, and minimum 0.081 kg C m^{-2} yr^{-1}

In addition Fig. 8 shows the frequency distribution of the simulated LAI values. The mean LAI for the boreal forests 9.26 with a standard deviation of 2.12. For 98.8% of the grid elements the values range from 7.5 to 12.5. In comparison Schulze (1982) collected estimations for LAI in a range between 7.4 and 9.4 for evergreen temperate coniferous forests and 7.0 to 19.0 for boreal forests. Simulation of LAI in cold deciduous forests resulted in a mean of 4.54, with standard deviation 1.23 and 98.8% ranging from 2.0 to 7. Schulze presented similar values for deciduous forests between 2.4 and 7.9.

Results along climatic gradients

In order to verify some of the climate responses of the model, we compared measured productivities and biomasses along climatic gradients with model output. As shown in Fig. 9 there is an increase of NPP with rising
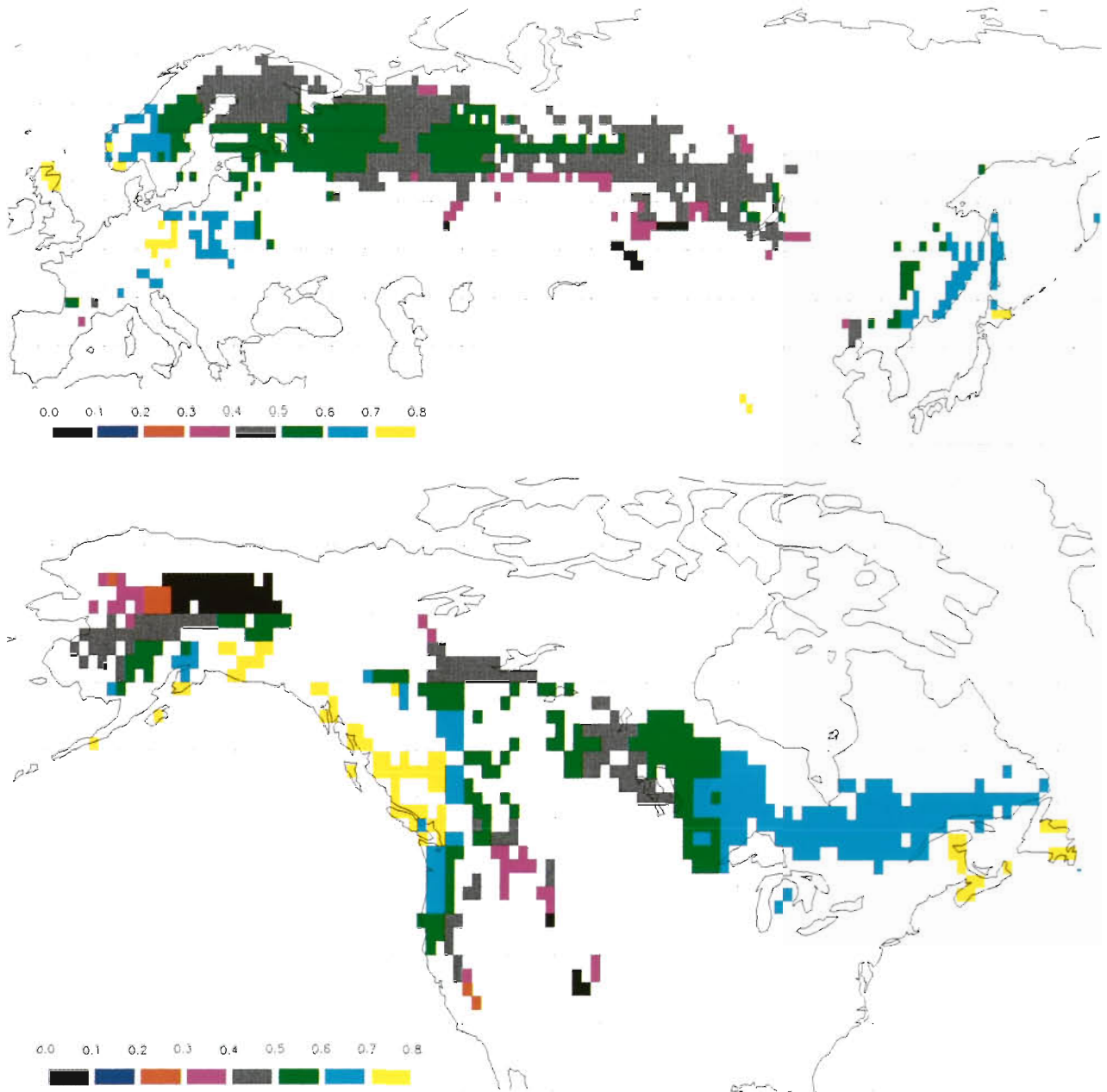
Fig. 5. Regional *NPP* distribution of vegetation type 8 (kg C m^{-2} yr^{-1}). Grid lines: 5° × 5°

latitude from 42 to 49° N at longitudes 142 to 144° W according to both the model results and the measured values reported by Vogt et al. (1982) and Webb et al. (1983). The annual sum of precipitation also increases in this south-north transect implying that the impact of this climate factor on net primary production is well reproduced by the model. These data were measured ·in the Pacific Northwest of the United States.

Additionally we compared the biomasses calculated for the boreal forests (type 8) with the biomass inventory data for Canada (Kurz et al. 1992). The highest biomasses are found on the Pacific coast. The biomass decreases from the Cordilleran, in western Canada, to central Canada where the lowest biomass was detected. In eastern Canada and on the Atlantic coast the forest's biomass increases again. This is qualitatively well reproduced by the model.

Comparing the absolute biomasses for Canadian boreal forests the calculated values are 3 times higher than the area averages of the measurements.

The absolute biomasses, however, are not directly comparable. While FBM calculates the total living bio-
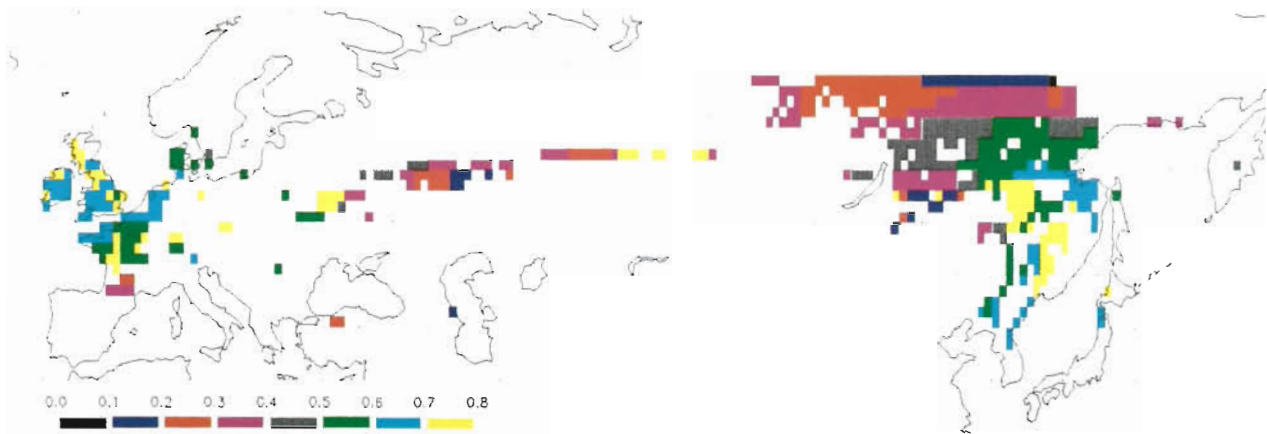
Fig. 6. Regional *NPP* distribution of vegetation type 11 (kg C m^{-2} yr^{-1}). Grid lines: 5° × 5°

mass of a natural climax forest the data derived from the biomass inventories refer to above-ground biomass of managed forests in a variable range of age classes. Due to management and natural fires the Canadian boreal forests are on average younger than the modeled climax forest. Nevertheless the trend caused by the climatic gradient is simulated by the model.

Seasonality

As described before our model was designed to simulate seasonal exchange fluxes of CO_2. At any time the fluxes are determined by external climatic and edaphic conditions as well as by the internal state of compartment sizes. Therefore the seasonality of the C compartment sizes will have an important impact on the fluxes, especially the GC compartment with its relatively high annual fluctuations.

In deciduous vegetation types rapid changes occur in the photosynthetically active fraction of GC at the transition from phase V to phase I and during the build-up of leaves in phase I as well as in phase IV (leaf shedding). The timing of the phase transitions V → I and III → IV can therefore be regarded as benchmarks for the reproduction of seasonal developments by the model. In Fig. 7 the regional distribution of leaf-shooting time in deciduous forests as predicted by FBM is depicted. Generally the beginning of the unfolding of leaves occurs in lower latitudes earlier than in higher latitudes. In northeastern Asia, a region with a late start of the vegetation period attracts attention. According to Walter & Breckle (1986) this region is characterized by an extreme continental climate with very low temperatures in winter.

For some European locations the model results can be compared with observations of the phenology. In Table 6 observations of leaf shooting times from a
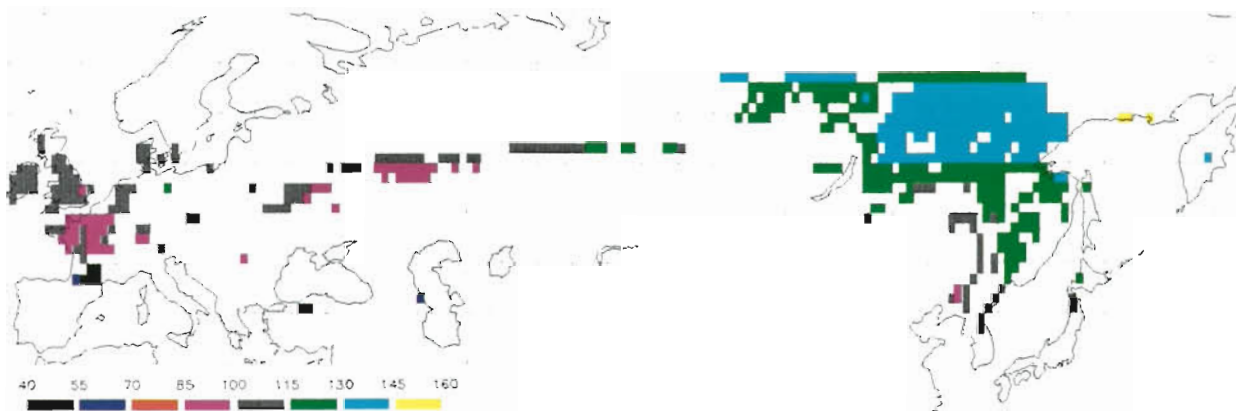

Fig. 7. Distribution of calculated leaf shooting dates of vegetation type 11. Grid lines: 5° × 5°
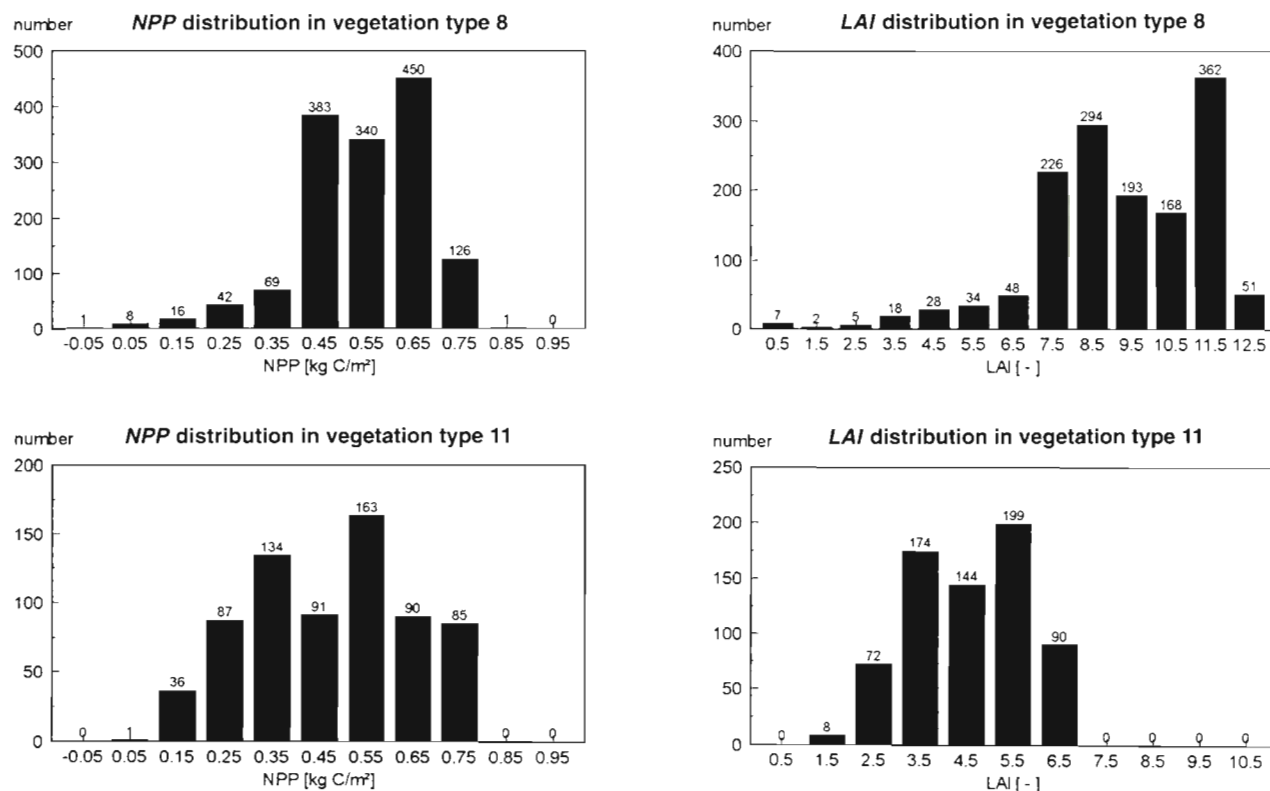
Fig. 8. Frequency distribution of *NPP* and projected *LAI* for vegetation types 8 and 11

group of phenological gardens at different locations (published by Schnelle 1985) are compared with model results. Observed leaf shooting days are the means of the observations of beech, oak, larch, poplar and birch trees for the period 1973 to 1982. These results show

Fig. 9. Calculated and measured *NPP* gradient and annual precipitation gradient. Measured *NPP* values from Vogt et al. (1982) and Webb et al. (1983)

that the very general flux-balance criterion for phase switching used in FBM provides a reasonable reproduction of the observed phenophases. The model tends to predict leaf shooting a little too early. It should be stressed that the model was not calibrated to reproduce the observed phenology. Therefore we conclude that the results [mean absolute error of 14 (9) d] are quite satisfactory. Considering the fact that we describe ecosystems it should be mentioned that some herbaceous plants and shrubs like elder (*Sambucus* sp.) and anemone in the understorey of forests unfold their leaves earlier to utilize full sunlight before the taller trees shade the ground, a fact which should be accounted for by the model. In order to demonstrate the sensitivity of the system with respect to temperature effects on photosynthesis, leaf shooting days from a simulation run calibrated with an increased minimum temperature (see Eq. 16 and Table 4) for net photosynthesis (from 0 to 5 °C) are given in brackets in Table 6.

Phenological data for eastern North America are available from Schwartz & Marotz (1986). They present the average of the first leaf emergence of *Syringa chinensis* in the time period 1961 to 1980. A comparison between the observations and the model results is given in Table 7. The model results fit well with the time range given by these observations. It seems that
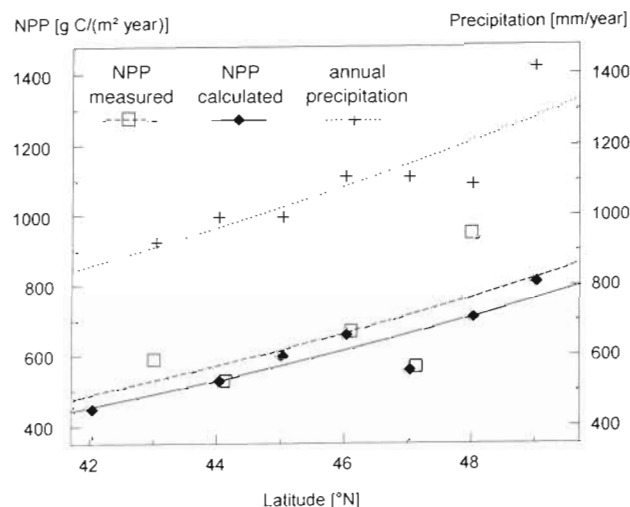
Table 6. Comparison of observed leaf shooting dates (10 yr range of single-species means in parentheses) with model results (results of a sensitivity study in parentheses, see text for details), vegetation type 11 (Julian days)

International phenological garden	Location	Leaf shooting date	
		Observed	Calculated
Vollebekk, Oslo Ås, Norway	10° E, 59° N	134 (124–138)	115 (124)
Ekebo, Lund-Svalöf, Sweden	13° E, 56° N	115 (107–123)	105 (118)
Tylstrup, Aalburg, Denmark	9° E, 57° N	128 (127–130)	111 (122)
Headley Park, London-Farnham, England	1° W, 51° N	121 (105–133)	111 (111)
Valentia Observat, Kerry, Ireland	10° W, 51° N	115 (92–123)	106 (111)
Johntown Castle, Wexford, Ireland	6° W, 52° N	118 (105–125)	105 (112)
Nat. Bot. Gardens, Dublin, Ireland	6° W, 53° N	107 (97–114)	110 (118)
Melle, Gent, Belgium	3° E, 50° N	116 (89–127)	100 (109)
Michamps, Basogne, Belgium	5° E, 51° N	132 (119–146)	105 (113)
Trier, Germany	6° E, 50° N	115 (104–119)	106 (114)
Rinn, Innsbruck, Austria	11° E, 47° N	127 (120–132)	101 (103)

Table 7. Comparison of observed first leaf emergence date with the model results for vegetation type 11 (Julian days)

Location	Leaf shooting date	
	Observed average	Calculated
90° W, 38° N	75–80	78
87° W, 39° N	80–85	81
87° W, 40° N	90–95	93
81° W, 41° N	95–100	96
85° W, 42° N	95–100	94
91° W, 42° N	95–100	91
86° W, 42° N	100–105	93
84° W, 43° N	110–120	111

the date of the first leaf of *S. chinensis* corresponds in a better way with the shooting day simulated by the model.

DISCUSSION

The model described here was intended to give a simple representation of the internal dynamics of the C compartments in terrestrial ecosystems. A second focus was directed on the climate dependence of the C fluxes in the ecosystems. The model, developed in the tradition of global carbon cycle modeling, has a higher level of aggregation than currently available stand-level ecosystem models (Ågren et al. 1991). From the model outputs on the seasonality of deciduous forests (see 'Results — Seasonality') it can be concluded that the concept of separating forbidden and allowed regions in the GC-RC phase space by the use of allometric relations together with the concept of switching phenophases according to the C balance, maximizing C assimilation, lead to satisfactory results. In the present state FBM includes preliminary representations of soil water dynamics and soil respiration. More detailed submodels for these processes are presently under development. Besides the internal C dynamics and climatic control of ecosystem performance nitrogen cycling is known to interplay substantially with C fluxes. The modulation of site quality by N availability already included in TEM will be incorporated into FBM in the future.

For model calibration we developed a set of rules for the derivation of a characteristic climate of a specified vegetation type. This method provides an alternative to the calibration of a model at a single site which has been applied by the authors of TEM. In future these different concepts for calibration and the resulting model responses can be compared to each other.

The simulation runs for boreal and cold deciduous forests calibrated for a characteristic climate predict distributions of biomass, leaf area index and primary production which fit fairly well the variability of these characteristics reported in the literature. In the frame of this model behaviour the effects of CO_2 partial pressure, temperature and soil water availability on the different fluxes (modeled with exchangeable modules for the single fluxes) will be studied in the near future in order to adress questions of ecosystem performance under changing climatic conditions.

As demonstrated for vegetation type 8, boreal forests, total *NPP* varies with the calibration parameter for the primary production in the characteristic climate. This result illustrates that model calculations of the global carbon cycle depend strongly on the estimates of *NPP* or parameters of the comparable structural relevance for the climax state characteristic mean stands. In this respect there is no difference between TEM and FBM. Especially with respect to boreal forests the estimates of biomass-density and net primary production currently are a matter of intensive debate (Wisniewski & Sampson 1993).

To discuss qualitatively the sensitivity of FBM results on the choice of its input parameters (Tables 4 & 5) it is useful to distinguish 3 groups of parameters:

(1) Ecological estimates on annual flux integrals such as *GPP*, autotrophic respiration of *GC* and *RC* which are target values of the calibration procedure.

(2) Ecophysiological parameters, defining the shape of the flux equations (e.g. Q_{10} values, initial quantum yield, and allometric relations).

(3) Free parameters (rate coefficients of the flux equations which are determined in the calibration routine by the condition to meet the target values of group 1).

The effect of changes of parameters of group 2 on the equilibrium simulation of a vegetation type according to its averaged annual flux integrals (e.g. as *NPP*, averaged over all pixels) is compensated by the calibration procedure, while one would expect changes in regional *NPP* distribution and the seasonal course of fluxes and state variables. In 'Results — Seasonality' such a parameter variation was performed by increasing the minimum temperature of net photosynthesis from 0 to 5 °C. The changes in phenology as documented in Table 6 were relatively small (about 10 d in shooting time).

On the other hand, changes of parameters in group 1 will cause both a corresponding change in the annual flux integrals averaged over the whole vegetation type as well as a change in regional distributions and seasonality. A quantitative sensitivity analysis referring to the influence of the various parameters determining the model equations will be published in a future paper.

The results presented for steady-state ecosystem performance, i.e. climax forests, give us some confidence that the model produces plausible results. The outputs (presented in the 'Results') can be seen as a contribution to model corroboration in the sense of Swartzman & Kaluzny (1987). Beyond the reproduction of exchange fluxes in climax vegetation the model structure allows for a description of growth dynamics and therefore the simulation of non-steady-state vegetation. Generally the model qualitatively correct reproduces growth periods in the time frame of some decades to more than 100 yr for forest ecosystems (Janecek et al. 1989, Kindermann et al. 1993). The model behaviour in non-steady-state situations will be discussed in detail in a future paper.

From the results of the simulated biomass, net primary production, phenology (see 'Results'), and the seasonal course of the exchange fluxes (Kindermann et al. 1993) it can be concluded that the model structure based on the determination of phenophases by external climatic conditions as well as the internal state of the living system (here given by the relative size of the compartments and their relation to functional interdependencies captured in the allometric relation) is appropriate for the description of short- and long-term dynamics in carbon exchange fluxes. Thus, closing the cycle to Goethe's (1790) remark cited at the beginning, it can be concluded that both external climatic conditions and internal mechanisms are to be considered when modeling ecosystem CO_2 exchanges.

Appendix 1

(A) Determination of the switching function *S*

In phase II the system is restricted to follow the allocation curve $\Omega(GC)$. This restriction determines the proportion *S* of newly formed assimilates to be distributed to compartment *GC*. The remaining proportion $1 - S$ of C_{ASS} fills the compartment *RC* ($0 \leq S \leq 1$).

If, however, the system is to follow the allometric relation between *RC* and *GC*, as given in Eq. (1), the derivative d*RC*/d*GC* as calculated from the division of Eq. (3) by Eq. (4)

$$\frac{dRC}{dGC} = \frac{(1-S) \cdot C_{ASS} - C_{RA} - C_{RS}}{S \cdot C_{ASS} - C_{GA} - C_{GS}} \quad (A1)$$

must be equal to the derivative of Eq. (1), $d\Omega/dGC$. Therefore we solve Eq. (A1) for *S* substituting d*RC*/d*GC* on the left side by $d\Omega/dGC$

$$S = \frac{C_{ASS} - C_{RA} - C_{RS} + \dfrac{d\Omega}{dGC} \cdot (C_{GA} - C_{GS})}{C_{ASS} \cdot \left(\dfrac{d\Omega}{dGC} + 1\right)} \quad (A2)$$

Inserting *S* in Eq. (4) gives:

$$\frac{dGC}{dt} = \frac{C_{ASS} - C_{RA} - C_{RS} - C_{GA} - C_{GS}}{\dfrac{d\Omega}{dGC} + 1} \quad (A3)$$

Appendix 1 (continued)

(B) Determination of GC and RC dynamics during phase V

In phase V the system is restricted to follow the curve $\Theta(GC)$. In analogy to Appendix 1A, we define L as the fraction of the total loss ($-C_{RA} - C_{BS}$, no autotrophic respiration from GC in this phase) coming from the GC compartment. Thus, we have the following differential equations:

$$\frac{dGC}{dt} = L \cdot (-C_{RA} - C_{BS}) \tag{A4}$$

$$\frac{dRC}{dt} = (1 - L) \cdot (-C_{RA} - C_{BS}) \tag{A5}$$

Again, the derivative dRG/dGC is to follow $\Theta(GC)$, from which we can determine L as

$$L = \frac{1}{1 + \dfrac{d\Theta}{dGC}} \tag{A6}$$

(C) Determination of the actual phenophase of deciduous vegetation in the case of station data

To ensure stable trajectories when using actual daily climate we specify the minimum number of days that a certain condition must hold before the system changes to another phase. If ΔBC becomes negative, the system will change from phase II to phase III, but only if this condition holds for Δ_{ab} successive days, it will change to phase IV. Similarly, Δ_{sh} consecutive days with $\Delta BC > 0$ are needed in phase V to initiate leaf shooting (phase I). The 'day counters' τ_{ab} and τ_{sh} are incremented in phases III and V and reset to 0 in phases I and IV, respectively. All conditions and incrementations are summarized in Table A1 (overleaf). For the simulation runs of this paper Δ_{ab} and Δ_{sh} are set equal to 1 because of the smooth course of the driving variables.

(D) Calculation of climate variables

Derivation of daily from monthly climate values

To obtain daily values from the monthly mean data of temperature and precipitation (e.g. as given by Shea 1986) we developed an iterative numerical interpolation algorithm, which preserves exactly the monthly mean values and produces a smooth time course.

In every iteration the number of mean values is doubled. In the first step 12 monthly values are splitted into 24 values. The idea of the algorithm is to divide the e.g. monthly values M_m into $p_m \cdot M_m$ and $(1 - p_m) \cdot M_m$ with $0 < p_m < 1$. p_m is calculated according to the ratio of the neighbouring M-values:

$$p_m = (1 - v) \cdot \left(\frac{M_{m-1}}{M_{m-1} + M_{m+1}}\right) + \frac{v}{2} \tag{A7}$$

where v is a damping variable between 0 and 1 For $v = 0$ we obtain the maximum influence of the ratio on p_m ($0 < p_m < 1$) whereas for $v = 1$ p_m becomes constant ($p_m = 1/2$). This iteration is repeated 6 times resulting in $12 \times 2^6 = 768$ values which are distributed over 365 (366) days. In contrast to extended (integral-preserving) algebraic interpolations this algorithm inherently avoids negative values of precipitation. A typical value for v is 0.7

Simulation of hourly temperature and light intensity

As the program executes a 24 h simulation, temperature and light follow a diurnal cycle. In the minimum data set used in FBM the diurnal cycle in temperature is estimated from the mean daily temperature T_d and the difference between minimum and maximum daily temperatures ΔT (Table 4) using a cosine function of time which is shifted so that the temperature follows the light with a 2 h delay:

$$T(t) = T(t_d, t_h) = T_d(t_d) + \frac{\Delta T}{2} \cdot \cos\left(\pi \frac{t_h - 14}{12}\right) \tag{A8}$$

The incoming photosynthetically active radiation (PAR) at any grid element and day of the year and time of the day is calculated from the theoretical formulas by Richter (1985). In the minimum data set the effect of cloudiness is neglected while the atmospheric absorption under clear sky conditions was considered. k_{atm} refers to clear sky conditions. An increase in k_{atm} due to an assumed constant cloudiness would tend to reduce the plant production, but would be nearly compensated by the calibration procedure, since α is increased correspondingly.

$$I(t) = I(t_d, t_h) = \begin{cases} I_{max} \cdot \theta(t) \cdot e^{-\frac{k_{atm}}{\theta(t)}} & \text{if } \theta(t) \geq 0 \\ 0 & \text{otherwise} \end{cases} \tag{A9}$$

$$\theta(t) = \theta(t_d, t_h) = \sin\lambda \cdot \sin\delta + \cos\lambda \cdot \cos\delta \cdot \cos\left(\pi \frac{t_h - 12}{12}\right) \tag{A10}$$

$$\delta(t) = \delta(t_d) = -0.408 \cdot \cos\left(\pi \frac{t_d + 10}{182.5}\right) \tag{A11}$$

Daylength:

$$D(t) = D(t_d) = \frac{24}{\pi} \arccos[-\tan\lambda \cdot \tan\delta(t_d)] \tag{A12}$$

where D is daylength (h); I_{max} is maximum incoming PAR (W m^{-2}); k_{atm} is atmospheric absorption coefficient ($k_{atm} = 0.12$); T_d is mean daily temperature (K); t_d is day of year (d); t_h is time of day (h); δ is declination of the sun (rad); λ is geographical latitude (rad); and θ is sine of elevation of the sun.

Table A1 (see Appendix 1C). Conditions determining the phenophase

Phase I: deciduous and evergreen type	Phase II: deciduous and evergreen type	Phase III: deciduous and evergreen type	Phase IV: deciduous type	Phase V: deciduous type
		Conditions		
$\Delta BC > 0 \wedge$	$\Delta BC > 0 \wedge$	$\Delta BC \leq 0$	starts: $\tau_{ab} = \Delta_{ab}$	
$RC = \Omega(GC)$	$RC = \Omega(GC)$	–	lasts: $RC < \Theta(GC)$	$RC = \Theta(GC)$
$\wedge \, \tau_{sh} = \Delta_{sh}$	–	$\wedge \, \tau_{ab} < \Delta_{ab}$	–	$\wedge \, \tau_{sh} < \Delta_{sh}$
		Calculations		
$\tau_{ab} = 0$	–	If $(\Delta BC_{cold} < 0)$	$\tau_{sh} = 0$	If $(\Delta BC > 0)$
		then $\tau_{ab} = \tau_{ab} + 1$		then $\tau_{sh} = \tau_{sh} + 1$
		else $\tau_{ab} = 0$		else $\tau_{sh} = 0$

Appendix 2. Matthews' vegetation types (1983), based on the physiognomic UNESCO classification (1973), modified according to Schmithüsen (1976)

No.	Name	No.	Name
1.	Tropical evergreen forest, mangrove forest	20.	Evergreen broadleaved shrubland/thicket, dwarf-shrubland
2.	Tropical/subtropical evergreen seasonal broadleaved forest	21.	Evergreen needleleaved/microphyllous shrubland/thicket
3.	Subtropical evergreen rainforest	22.	Drought-deciduous shrubland/thicket
4.	Temperate/subpolar evergreen rainforest	23.	Cold-deciduous subalpine/subpolar shrubland, dwarf shrubland
5.	Temperate evergreen seasonal broadleaved forest, summer rain	24.	Tropical xeromorphic shrubland / dwarf shrubland
6.	Evergreen broadleaved sclerophyllous forest, winter rain	25.	Temperate dwarf shrubland
		26.	Tropical dry xeromorphic shrubland / dwarf shrubland
7.	Tropical/subtropical evergreen needleleaved forest	27.	Arctic/alpine tundra, mossy bog
8.	Temperate/subpolar evergreen needleleaved forest		
9.	Tropical/subtropical drought-deciduous forest		
10.	Cold-deciduous forest, with evergreens	30.	Tropical grassland with woody tree cover / humid savanna
11.	Cold-deciduous forest, without evergreens	31.	Tropical grassland / dry savanna
12.	Xeromorphic forest/woodland	32.	Tropical grassland / thorn savanna
13.	Evergreen broadleaved sclerophyllous woodland	33.	Tropical grassland / small-leaved thorn-tree woodland
14.	Evergreen needleleaved woodland	34.	Temperate grassland with woody tree cover (C_3)
15.	Tropical/subtropical drought-deciduous woodland	35.	Temperate grassland with woody tree cover (C_4)
16.	Cold-deciduous woodland	36.	Temperate grassland/steppe, prairie (C_3)
		37.	Temperate grassland/steppe, prairie (C_4)

Appendix 3. Assignment of soil types from texture-drainage combinations given by Wilson & Henderson-Sellers (1985) and soil properties (Donahue et al. 1977, Clapp & Hornberger 1978). Rooting depth is assumed to be 1 m

FBM soil type	Texture	Drainage	FC (mm)	PWP (mm)
1. Sand	Coarse	Good	140	25
2. Sandy loam	Medium	Good	175	40
3. Silt clay	Fine	Good	265	120
4. Loam	Coarse	Impeded	250	100
5. Clay loam	Medium	Impeded	290	145
6. Clay	Fine	Impeded	335	198
7. Wetlands	–	Poor	–	–

Appendix 4. List of variables

Symbol	Description	Unit
a_T, a_{SW}	Adjustment coefficients	$-$, s^{-1}
BC	Carbon in living biomass	$kg\ C\ m^{-2}$
ΔBC	Daily increment of BC	$kg\ C\ m^{-2}$
ΔBC_{cold}	Potential daily increment of BC (without water limitation)	$kg\ C\ m^{-2}$
C_{ASS}	Carbon assimilation (i.e. gross photosynthesis)	$kg\ C\ m^{-2}\ s^{-1}$
C_{CER}	Carbon exchange rate (i.e. net photosynthesis)	$kg\ C\ m^{-2}\ s^{-1}$
C_{xy}	Carbon flux from compartment x to y	$kg\ C\ m^{-2}\ s^{-1}$
FC	Field capacity	mm
GC	Carbon compartment: leaf, feeder roots and storage	$kg\ C\ m^{-2}$
GC_{max}	Climax carbon content of GC	$kg\ C\ m^{-2}$
GPP	Gross primary production	$kg\ C\ yr^{-1}\ m^{-2}$
$h_1(I, LAI)$	Light dependent term of carbon assimilation	$-$
$h_2(T)$	Temperature dependent term of carbon assimilation	$-$
$h_3(SW)$	Soil water dependent term of carbon assimilation	$-$
I	Photosynthetic active radiation (PAR), top of the canopy	$W\ m^{-2}$
$I_{can}(L)$	PAR in the canopy at leaf layer L	$W\ m^{-2}$
k	Extinction coefficient in Beer's law	$m^{-2}\ m^2$
L	Cumulative leaf area index	$m^2\ m^{-2}$
LAI	Leaf area index ($LAI = SLA \cdot GC/2$)	$m^2\ m^{-2}$
LpG	Litter production of the GC compartment	$kg\ C\ m^{-2}\ s^{-1}$
LpR	Litter production of the RC compartment	$kg\ C\ m^{-2}\ s^{-1}$
NPP	Net primary production	$kg\ C\ yr^{-1}\ m^{-2}$
PWP	Permanent wilting point	mm
q_{RG}	Temperature response factors for soil respiration	$-$ or $°C^{-1}$
RC	Carbon compartment: stem and roots	$kg\ C\ m^{-2}$
RC_{max}	Climax carbon content of RC	$kg\ C\ m^{-2}$
$ResG$	Annual integral of respiration fluxes, climax state, GC	$kg\ C\ m^{-2}\ yr^{-1}$
$ResR$	Annual integral of respiration fluxes, climax state, RC	$kg\ C\ m^{-2}\ yr^{-1}$
RG	Soil types with respect to heterotroph respiration	
S	Fraction of total assimilate allocated to GC	
SC	Carbon compartment: soil organic carbon, humus and litter	$kg\ C\ m^{-2}$
SC_{max}	Climax carbon content of SC	$kg\ C\ m^{-2}$
SLA	Specific leaf area	$m^2\ kg^{-1}\ C$
SW	Water compartment: soil water content	mm
T	Actual air temperature	K
T_0	Reference temperature for autotroph respiration ($T_0 = 293$)	K
T_{max}	Maximum temperature of net photosynthesis	K
T_{min}	Minimum temperature of net photosynthesis	K
T_{opt}	Optimum temperature of net photosynthesis	K
W_{AS}	Daily precipitation	$mm\ d^{-1}$
W_{PET}	Potential evapotranspiration (Thornthwaite)	$mm\ d^{-1}$
W_{Runoff}	Runoff (surface runoff and drainage)	$mm\ d^{-1}$
W_{SA}	Actual evapotranspiration	$mm\ d^{-1}$
α, β, γ, δ, ε, η	Calibration parameters	$kg\ C\ m^{-2}\ s^{-1}$, s^{-1}
Φ	Initial quantum yield	$kg\ C\ W^{-1}$
Ω	Allometric relation: $RC = \Omega(GC)$ (right confinement)	
Θ	Allometric relation: $RC = \Theta(GC)$ (left confinement)	
κ	Exponential parameter of allometric relations	$-$
ν	Parameter in $\Theta(GC)$ relation	$[(kg\ C\ m^{-2})^{1/\kappa}]$
ξ	Parameter in $\Omega(GC)$ relation	$[(kg\ C\ m^{-2})^{1/\kappa}]$
ω	Exponential parameter for autotroph respiration	K^{-1}
τ_{ab}	Time delay, leaf abscission	d
τ_{sh}	Time delay, leaf shooting	d
τ_{IV}	Duration of phase IV	d

LITERATURE CITED

Ågren, G. I., McMurtrie, R. E., Parton, W. J., Pastor, J., Shugart, H. H. (1991). State-of-the-art of models of production-decomposition linkages in conifer and grassland ecosystems. Ecol. Appl. 1(2): 118–138

Ajtay, G. L., Ketner, P., Duvigneaud, P. (1979). Terrestrial primary production and phytomass. In: Bolin, B. et al. (eds.) The global carbon cycle. SCOPE 13. J. Wiley & Sons, Chichester, p. 129–181

Björkman, O. (1981). Response to different quantum flux densities. In: Lange, O. L., Nobel, P. S., Osmond, C. B., Ziegler, H. (eds.) Physiological plant ecology I. Responses to the physical environment. Encyclopedia of plant physiology, New Series 12a. Springer, Berlin, p. 57–107

Box, E. O. (1981). Macroclimate and plant forms: an introduction to predictive modeling in phytogeography. Junk, The Hague

Box, E. O., Meentemeyer, V. (1991). Geographic modeling and modern ecology. In: Esser, G., Overdieck, D. (eds.) Modern ecology. Basic and applied aspects. Elsevier, Amsterdam, p. 773–804

Ceulemans, R. J., Saugier, B. (1991). Photosynthesis. In: Raghavendra, A. S. (ed.) Physiology of trees. J. Wiley & Sons, New York, p. 22–50

Clapp, R. B., Hornberger, G. M. (1978). Empirical equations for some soil hydraulic properties. Water Resour. Res. 14(4): 601–604

Dixon, K. R. (1976). Analysis of seasonal leaf fall in north temperate deciduous forests. Oikos 27: 300–306

Donahue, R. L., Miller, R. W., Shickluna, J. C. (1977). Soils — an introduction to soils and plant growth. Prentice-Hall, Englewood Cliffs, NJ

Ehleringer, J., Mooney, H. A. (1983). Productivity of desert and Mediterranean climate plants. In: Lange, O. L., Nobel, P. S., Osmond, C. B., Ziegler, H. (eds.) Physiological plant ecology IV. Ecosystem processes: mineral cycling, productivity and man's influence. Encyclopedia of plant physiology, New Series 12a. Springer, Berlin, p. 205–231

Ellenberg, H., Mayer, R., Schauermann, J. (eds.) (1986). Ökosystemforschung — Ergebnisse des Sollingprojekts 1966–1986. Eugen Ulmer Verlag, Stuttgart

Enting, I. G., Mansbridge, J. V. (1989). Seasonal sources and sinks of atmospheric CO_2: direct inversion of filtered data. Tellus 41B: 111–126

Esser, G. (1987). Sensitivity of global carbon pools and fluxes to human and potential climatic impacts. Tellus 39B(3): 245–260

Esser, G. (1991). Osnabrück Biosphere Model: structure, construction, results. In: Esser, G., Overdieck, D. (eds.) Modern ecology. Basic and applied aspects. Elsevier, Amsterdam, p. 679–709

FAO/UNESCO (1971–1979). Soil map of the World I–IX. 1:5000000. UNESCO, Paris

Farquhar, G. D., Caemmerer, S. von, Berry, J. A. (1980). A biochemical model of photosynthetic CO_2 assimilation in leaves of C_3 species. Planta 149: 78–90

Fung, I. Y., Tucker, C. J., Prentice, K. C. (1987). Application of advanced very high resolution radiometer vegetation index to study atmosphere-biosphere exchange of CO_2. J. geophys. Res. 92(D3): 2999–3015

Gifford, R. M. (1993). Implications of CO_2 effects on vegetation for the global carbon budget. In: Heimann, M. (ed.) The global carbon cycle. Springer, Berlin, p. 159–199

Goethe, J. W. (1790). Vorarbeiten zu einer Physiologie der Pflanzen. In: Schriften zur Botanik und Wissenschaftslehre, dtv-Gesamtausgabe Band 39. Deutscher Taschenbuch Verlag, Nördlingen (1963)

Gorham, E. (1991). Northern peatlands: role in the carbon cycle and probable responses to climatic warming. Ecol. Appl. 1(2): 182–195

Goudriaan, J, Ketner, P. (1984). A simulation study for the global carbon cycle, including man's impact on the biosphere. Clim. Change 6(2): 167–192

Hadley, N. F., Szarek, S. R. (1981). Productivity of desert ecosystems. BioSci. 31(10): 747–753

Heath, L. S., Kauppi, P. E., Burschel, P., Gregor, H. D., Guderian, R., Kohlmaier, G. H., Lorenz, S., Overdieck, D., Scholz, F., Thomasius, H., Weber, M. (1993). Contribution of temperate forests to the world's carbon budget. In: Wisniewski, J., Sampson, R. N. (eds.) Terrestrial biospheric fluxes: quantification of sinks and sources of CO_2. Kluwer Academic, Dordrecht, p. 55–70

Heimann, M, Keeling, C. D. (1989). A three-dimensional model of atmospheric CO_2 transport based on observed winds: 2. Model description and simulated tracer experiments. In: Peterson, D. H. (ed.) Aspects of climate variability in the Pacific and the western Americas. Geophys. Monogr. 55: 237–275

Holdridge, L. R. (1947). Determination of world plant formations from simple climatic data. Science 105: 367–368

Janecek, A., Benderoth, G., Lüdeke, M. K. B., Kindermann, J., Kohlmaier, G. H. (1989). Model of the seasonal and perennial carbon dynamics in deciduous-type forests controlled by climatic variables. Ecol. Modelling 49: 101–124

Jarvis, P. G., Leverenz, J. W. (1983). Productivity of temperate, deciduous and evergreen forests. In: Lange, O. L., Nobel, P. S., Osmond, C. B., Ziegler, H. (eds.) Physiological plant ecology IV. Ecosystem processes: mineral cycling, productivity and man's influence. Encyclopedia of plant physiology, New Series 12a. Springer, Berlin, p. 233–280

Keeling, C. D., Bacastow, R. B., Carter, A. F., Piper, S. (1989). A three-dimensional model of atmospheric co_2 transport based on observed winds: 1. Analysis of observational data. In: In: Peterson, D. H. (ed.) Aspects of climate variability in the Pacific and the western Americas. Geophys. Monogr. 55: 165–236

Kindermann, J., Lüdeke, M. K. B., Badeck, F.-W., Otto, R. D., Klaudius, A., Häger, Ch., Würth, G., Lang, T., Dönges, S., Habermehl, S., Kohlmaier, G. H. (1993). Structure of a global and seasonal carbon exchange model for the terrestrial biosphere. The Frankfurt Biosphere Model (FBM). Water Air Soil Pollut. 70: 675–984

Kira, T (1975). Primary production of forests. In: Cooper, J. P. (ed.) Photosynthesis and productivity in different environments. International Biological Programme 3. Cambridge University Press, Cambridge, p. 5–40

Kohlmaier, G. H., Benderoth, G., Klaudius, A., Janecek, A., Kindermann, J. (1989). Multifactorial interpretation of the amplitude increase of the seasonal atmospheric CO_2 cycle at the Mauna Loa Station. In: World Meteorological Organisation (ed.) Extended abstracts of papers presented at the 3rd international conference on analysis and evaluation of atmospheric CO_2 data present and past. WMO/TD, No. 340, p. 274–279

Kohlmaier, G. H., Bröhl, H., Siré, E. O., Plöchl, M., Revell, R. (1987). Modelling stimulation of plants and ecosystem response to present levels of excess atmospheric CO_2. Tellus 39B: 155–170

Kohlmaier, G. H., Lüdeke, M., Janecek, A., Benderoth, G., Kindermann, J., Klaudius, A. (1991). Land biota, source or sink of atmospheric carbon dioxide: positive and negative feedbacks within a changing climate and land use development. In: Schneider, S. H., Boston, P. J. (eds.) Scientists

on Gaia. MIT Press, Cambridge, p. 223–239

Kohlmaier, G. H., Lüdeke, M., Kindermann, J., Klaudius, (1990). Kohlenstoffzyklus und Biosphäre: mögliche Entwicklungen und Strategien bei einer Klimaänderung. VDI-Berichte 809: 7–25

Kurz, W. A., Apps, M. J., Webb, T M., McNamee, P. J. (1992). The carbon budget of the Canadian forest sector: phase I. Information Report NOR-X-326, Forestry Canada, Northwest Region, Northern Forestry Centre, Edmonton. Alberta

Larcher, W. (1980). Physiological plant ecology. Springer, Berlin

Leemans, R., Cramer, W. P. (1991). The IIASA database for mean monthly values of temperature, precipitation and cloudiness on a global terrestrial grid. Research Report RR-91-18, International Institute for Applied Systems Analysis, Laxenburg, Austria

Lieth, H. (1975). Primary productivity in ecosystems: comparative analysis of global patterns. In: von Dobben, W. H., Lowe-McConnell, R. H. (eds.) Unifying concepts in ecology. Junk, The Hague, p. 76–88

Long, S. P., Drake, B. G. (1992). Photosynthetic CO_2 assimilation and rising atmospheric CO_2 concentrations. In: Baker, N. R., Thomas, H. (eds.) Crop photosynthesis: spatial and temporal determinants. Elsevier, Amsterdam, p. 69–103

Long, S. P., Jones, M. B., Roberts, M. J. (eds.) (1992). Primary productivity of grass ecosystems of the tropics and subtropics. Chapman & Hall, London

Matthews, E. (1983). Global vegetation and land use: new high-resolution data bases for climate studies. J. Clim. appl. Meteorol. 22(3): 474–487

Matthews, E. (1984). Global inventory of pre-agricultual and present biomass. Prog. Biometeorol. 3: 237–246

Medina, E., Klinge, H. (1983). Productivity of tropical forests and tropical woodlands. In: Lange, O. L., Nobel, P. S., Osmond, C. B., Ziegler, H. (eds.) Physiological plant ecology IV. Ecosystem processes: mineral cycling, productivity and man's influence. Encyclopedia of plant physiology, New Series 12a. Springer, Berlin, p. 281–303

Melillo, J M., McGuire, A. D., Kicklighter, D. W. (1993). Global climate change and terrestrial net primary production. Nature 363: 234–240

Monsi, M., Saeki, T (1953). Über den Lichtfaktor in den Pflanzengesellschaften und seine Bedeutung für die Stoffproduktion. Jap. J. Bot. 14: 22–52

Moore, B., Boone, R. D., Hobbie, J. E., Houghton, R. A., Melillo, J. M., Peterson, B. J., Shaver, G. R., Vörösmarty, C. J., Woodwell, G. M. (1979). A simple model for analysis of the role of terrestrial ecosystems. In: Bolin, B. (ed.) The global carbon budget. SCOPE 16. J Wiley & Sons, Chichester, p. 365–385

Olson, J., Watts, J. A. (1982). Major world ecosystem complexes ranked by carbon in live vegetation (map). NDP-017, Oak Ridge National Laboratory, Oak Ridge, TN

Post, W. M., Pastor, J., Zinke, P. J., Stangenberger, A. G. (1985). Global patterns of soil nitrogen storage. Nature 317: 613–616

Prentice, I. C., Cramer, W., Harrison, S. P., Leemans, R. (1992). A global biome model based on plant physiology and dominance, soil properties and climate. J. Biogeogr. 19: 117–134

Raich, J. W., Rastetter, E. B., Melillo, J. M., Kicklighter, D. W., Steudler, P. A., Peterson, B. J., Grace, A. L., Moore, B., Vörösmarty, C. J. (1991). Potential net primary productivity in South America: application of a global model. Ecol. Appl. 1(4): 399–429

Rasmussen, R. A., Khalil, M. A. K. (1986). Atmospheric trace gases: trends and distribution over the last decade. Science 232: 1623–1624

Reichle, D. E. (ed.) (1981). Dynamic properties of forest ecosystems. International Biological Programme 23. Cambridge University Press, Cambridge

Richter, O. (1985). Simulation des Verhaltens ökologischer Systeme. Mathematische Methoden und Modelle. Verlag Chemie, Weinheim

Rodin, L. E., Bazilevich, N. I., Rozov, N. N. (1972). Productivity of the world's main ecosystems. In: Productivity of world ecosystems. Proc. Seattle symp. 1972. Nat. Acad. Sci., Washington, DC, p. 13–26

Ruimy, A. (1991). Estimation de la production primaire nette continentale à partir de mesures satellitaires. D.E.A. Ecophysiologie, Univ. Paris XI

Running, S. W., Coughlan, J. C. (1988). A general model of forest ecosystem processes I. Hydrology balance, canopy gas exchange and primary production processes. Ecol. Modelling 42(2): 125–154

Ryan, M. G. (1991). Effects of climate on plant respiration. Ecol. Appl. 1(2): 157–167

Schlesinger, W. H. (1984). Soil organic matter: a source of atmospheric CO_2. In: Woodwell, G. M. (ed.) The role of terrestrial vegetation in the global carbon cycle: measurement by remote sensing. SCOPE 23. J. Wiley & Sons, Chichester, p. 111–127

Schmithüsen, J. (1968). Allgemeine Vegetationsgeographie. Lehrbuch der Allgemeinen Geographie 4. Walter de Gruyter, Berlin

Schmithüsen, J. (ed.) (1976). Atlas zur Biogeographie. Meyers Großer Physischer Weltatlas 8. Bibliographisches Institut, Mannheim

Schnelle, F. (1985). 10-jährige Mittel (Zeiträume 1963–1972 und 1973–1982) für 17 Phasen, die in 13 IPG beobachtet wurden. Arboreta Phaenologica 29: 12–28

Schulze, E.-D. (1982). Plant life forms and their carbon, water and nutrient relations. In: Lange, O. L., Nobel, P. S., Osmond, C. B., Ziegler, H. (eds.) Physiological plant ecology II. Water relations and carbon assimilation. Encyclopedia of plant physiology, New Series 12a. Springer, Berlin, p. 615–676

Schulze, E.-D., Kappen, L. (1975). Primary production of deserts. In: Cooper, J. P. (ed.) Photosynthesis and productivity in different environments. International Biological Programme 3. Cambridge University Press, Cambridge, p. 107–132

Schwartz, D. M., Marotz, G. A. (1986). An approach to examining regional atmosphere-plant interactions with phenological data. J. Biogeogr. 13: 551–560

Schwarzbach, M. (1974). Das Klima der Vorzeit. Eine Einführung in die Paläoklimatologie. Ferdinand Enke, Stuttgart

Shea, D. J. (1986). Climatological atlas: 1950–1979. Surface air temperature, precipitation, sea-level pressure, and sea-surface temperature (45° S–90° N). NCAR Technical Note 269+STR. National Center for Atmospheric Research, Boulder, CO

Swartzman, G. L., Kaluzny, S. P. (1987). Ecological simulation primer. Macmillan Publishing Company, New York

Tans, P. P., Fung, I. Y., Takahashi, T. (1990). Observational constraints on the global atmospheric CO_2 budget. Science 247: 1431–1438

Thornthwaite, C. W. (1948). An approach toward a rational classification of climate. Geogr. Rev. 38: 55–94

UNESCO (1973). International classification and mapping of vegetation. Ecology and Conservation 6. UNESCO, Paris

UNESCO (1981). Vegetation map of South America: explanatory notes. Natural Resources Research 17. UNESCO, Paris

UNESCO (1981). Vegetation map of Africa 1:5000000. UNESCO, Paris

UNESCO/FAO (1969). Carte de la végétation de la région Méditerranéenne. Étude écologique de la zone Méditerranéenne. Recherches sur la zone Aride 30. UNESCO, Paris

Vogt, K. A., Grier, C. C., Meier, C. E., Edmonds, R. L. (1982). Mycorrhizal role in net primary production and nutrient cycling in abies amabilis ecosystems in western Washington. Ecology 63: 370–380

Walter, H., Breckle, S.-W. (1983). Ökologische Grundlagen in globaler Sicht. Ökologie der Erde, 1. UTB für Wissenschaft, Große Reihe. Gustav Fischer, Stuttgart

Walter, H., Breckle, S.-W. (1984). Spezielle Ökologie der tropischen und subtropischen Zonen. Ökologie der Erde, Band 2. UTB für Wissenschaft, Große Reihe. Gustav Fischer, Stuttgart

Walter, H., Breckle, S.-W. (1986). Spezielle Ökologie der gemäßigten und arktischen Zonen Euro-Nordasiens.

Zonobiom VI-IX. Ökologie der Erde Band 3. UTB für Wissenschaft, Große Reihe. Gustav Fischer, Stuttgart

Walter, H., Breckle, S.-W. (1991). Spezielle Ökologie der gemäßigten und arktischen Zonen außerhalb Euro-Nordasiens. Zonobiom IV-IX. Ökologie der Erde, Band 4. UTB für Wissenschaft, Große Reihe. Gustav Fischer, Stuttgart

Webb, W. L., Lauenroth, W. K., Szarek, S. R., Kinerson, R. S. (1983). Primary production and abiotic controls in forests, grasslands, and desert ecosystems in the United States. Ecology 64(1): 134–151

Whittaker, R. H., Likens, G. E. (1975). The biosphere and man. In: Lieth, H., Whittaker, R. H. (eds.) Primary productivity of the biosphere. Springer, Berlin, p. 305–328

Wilson, M. F., Henderson-Sellers, A. (1985). A global archive of land cover and soils data for use in general circulation climate models. J. Climatol. 5: 119–143

Wisniewski, J., Sampson, R. N. (eds.) (1993). Terrestrial biospheric carbon fluxes: quantification of sinks and sources of CO_2. Kluwer Academic, Dordrecht

Woodward, F. I. (1987). Climate and plant distribution. Cambridge University Press, Cambridge